Desalination of High-salinity Water by Membranes

by

Aoran Gao

A thesis

presented to the University of Waterloo

in fulfillment of the

thesis requirement for the degree of

Master of Applied Science

in

Chemical Engineering

Waterloo, Ontario, Canada, 2016

Author's Declaration

I hereby declare that I am the sole author of this thesis. This is the true copy of the thesis, including any required final revisions, as accepted by my examiners.

I understand that my thesis may be made electronically available to the public.

Abstract

This study deals with the desalination of high-salinity water using membranes by pervaporation. The membrane performance was characterized with water flux and salt rejection. It was shown that a water flux of 1.6 kg/m^{2}h and almost complete salt rejection (99.9%) were achieved at 65℃. The water flux increased with an increase in temperature, and the temperature dependence of water flux obeyed an Arrhenius type of equation. The water flux decreased with an increase in the salinity of the feed solutions; increasing salt concentration from 1 to 20 wt% resulted in a 50% reduction in water flux, whereas the salt rejection was not influenced. The water flux varied with the type of the salts (i.e., NaCl, Na_2SO_4 and $MgCl_2$) in the feed water, but the salt rejection remained over 99.9%, regardless of salt types and concentrations. Batch operation (10 hours) of desalination was studied to investigate the permeation flux variation in pervaporation process. The permeation flux continuously decreased during the course of operation, and when there was 20 wt% of salts in the feed solution, the water flux was 30% lower than pure water flux. The permeation flux could be recovered after the membrane surface was rinsed by water flow.

In order to get an insight into water transport in the membrane, experiments were also carried out with membranes of different thicknesses. The water flux decreased with an increase in the membrane thickness from 39 to 88μm, and the membrane thickness dependence of water flux followed the Fick's law. Mass transport in the membranes was analyzed quantitatively. The apparent diffusion coefficient of water was shown to decrease with an increase in salt

concentration in the feed solution. The salt solubility in the membrane followed the order of $MgCl_2$>NaCl>Na_2SO_4, and the salt permeability in the membrane followed the order of NaCl>$MgCl_2$>Na_2SO_4. Moreover, the concentration profile within the membrane was also determined experimentally.

Acknowledgements

I would like to express my sincere appreciation and gratitude to my supervisor Professor Xianshe Feng for giving me such a great opportunity to study in University of Waterloo. His patience encouragement, constructive criticism and invaluable guidance always supported me during my Master's studies. This thesis would not have been possible without his unwavering guidance.

I would also like to express my gratitude to the examination committee for their advice and comments on my thesis.

I wish to thank all my colleagues from our group for all their assistance, support and advice in the past two years during my study, including Dr. Dihua Wu, Dr. Yifeng Huang, Boya Zhang, Shuixiu Lai, Bo Qiu. I also would like to thank Dr. Jingde Li for ASPEN data analysis.

I would like to give my special thanks to my parents for their encouragement, love, and support during my Master's studies.

I would like to thank all my best friends for their support and encouragement.

Table of Contents

List of Figures

List of Tables

Chapter 1

Introduction

1.1 Background

In the past few decades, water scarcity has become one of the most serious challenges globally in the society. Over 2.3 billion people on the Earth live in the water-stressed areas, and this number is expected to increase to 3.5 billion by 2025 [Elimelech and Phillip, 2011]. In order to maintain the sustainable development of economy and environment, Global Water Partnership was established in 1996 to develop Integrated Water Resources Management, focusing on the adjustment, management and development of water, land and related resources. Technologies for water desalination have been developed in two approaches: one is based on distillation, including multi-stage flash distillation and multiple-effect distillation; the other is membrane-based desalination, including nanofiltration, vacuum membrane distillation and reverse osmosis. In recent years, membrane separation processes become more and more popular in desalination because there is no phase change in the membrane processes (except pervaporation). As a result, the energy requirements are lower than that of the traditional distillation processes. Membrane processes are environmental friendly since the membranes are made of relatively simple and non-harmful materials. A large number of polymers can be used to prepare membranes. In general, a high salt rejection and permeation flux are required for desalination with membrane processes. Until now, RO has been one of the most important membrane processes for desalination in industrial scale. However, the wide spread use of RO process is restricted by the

ooperating conditions and high energy cost. To deal with high-salinity water, an extremely high operating pressure is needed in RO process. Comparing with RO, pervaporative desalination only to use a vacuum pump to induce water permeation and hence consumes less energy. Although pervaporation is normally used for separating a mixture of volatile components, water desalination by pervaporation may also work if suitable membranes are available.

The membranes used in this study were made of poly(ether block amide) (Pebax®) which is a hydrophilic polymer. Pebax is copolymer with soft and flexible segments, which make it useful in many areas, including medical, textile and membrane applications. The Pebax® polymer used in this work had high sorption of water vapor [Sabzi et al., 2014, Potreck et al., 2009, Sijbesma et al., 2008]. However, very little research is done related to Pebax for desalination applications. Therefore, the performance of Pebax membrane for desalination of high-salinity water was studied in this thesis work.

1.2 Objectives

This study dealt with the desalination of high-salinity water using membranes by pervaporation. The research consisted of the followings:

(1) To investigate the pervaporative separation performance of Pebax membrane for desalination of high-salinity water under different operating conditions (e.g. temperature, feed concentration).

(2) To study the mass transport of water and salt in the membrane in pervaporation process.

1.3 Thesis Outline

The thesis consists of five chapters as follows:

Chapter 1 introduces the thesis work and describes the objective of the research.

Chapter 2 reviews the principles of pervaporation and the mass transport mechanisms (e.g., solution-diffusion model and pore-flow model). This chapter also introduces the characteristics of Pebax polymer, as well as several other desalination processes.

Chapter 3 presents the experiment setup and the procedure for membrane preparation. The experimental work consisted of three prats. First, the water desalination process under pervaporation model was used to investigate the performance of Pebax membrane. Sorption and permeation experiments were then carried out to evaluate the influence of different salts in water on membrane performance. Multi-membrane layers was then used in the pervaporative desalination experiments to determine the concentration profile of the salts in the membrane.

Chapter 4 demonstrates the pervaporative performance of Pebax membrane for desalination of high-salinity water. A comparison of the separation performance between pervaporation and other desalination processes are also presented.

Lastly, Chapter 5 describes the general conclusions of this study. Based on the thesis research work, recommendations for future studies are also provided.

Chapter 2

Literature Review

Membrane separations have been widely used in the industry for the separation of gaseous and liquid mixtures. Compared with the existing separation technologies (e.g. rectification, distillation, or crystallization), membrane processes are not limited by opearting temperature and in general they have advantages in energy savings. In addition, membrane processes do not involve any chemical reactions, and therefore they are friendly to the environment. Moreover, membrane processes are generally more convenient and effective than traditional separation processes.

Pervaporation is a relatively new membrane separation process for liquid separation [Huang, 1991]. In recent years, pervaporation process has been widely used for dehydration of organic solvents. This chapter will present an overview of the principles of pervaporation, including the process fundamental and mass transport mechanism. In addition, the preparation of homogeneous membrane used in pervaporation will also be described.

2.1 Characteristics of pervaporation

Pervaporation is a relatively new membrane separation process similar to membrane distillation and reverse osmosis. The word ‘pervaporation’ is derived from the two steps of the process: (a) permeation through a membrane, (b) evaporation into the vapor phase. In this process on the permeate side, the membrane may be considered as a selective barrier between the liquid phase (feed) and vapor phase (permeate). The desired components in a liquid mixture pass through the membrane, and the permeated components are removed as vapor from the other side. The permeate vapor can be condensed and collected. Figure 2.1 shows a schematic diagram of the pervaporation process. The driving force for mass transport is the chemical potential gradient across the membrane. It can be created by a vacuum pump or an inert purge to maintain a vapor pressure of the permeate lower than the partial vapor pressure of the component on the feed side.

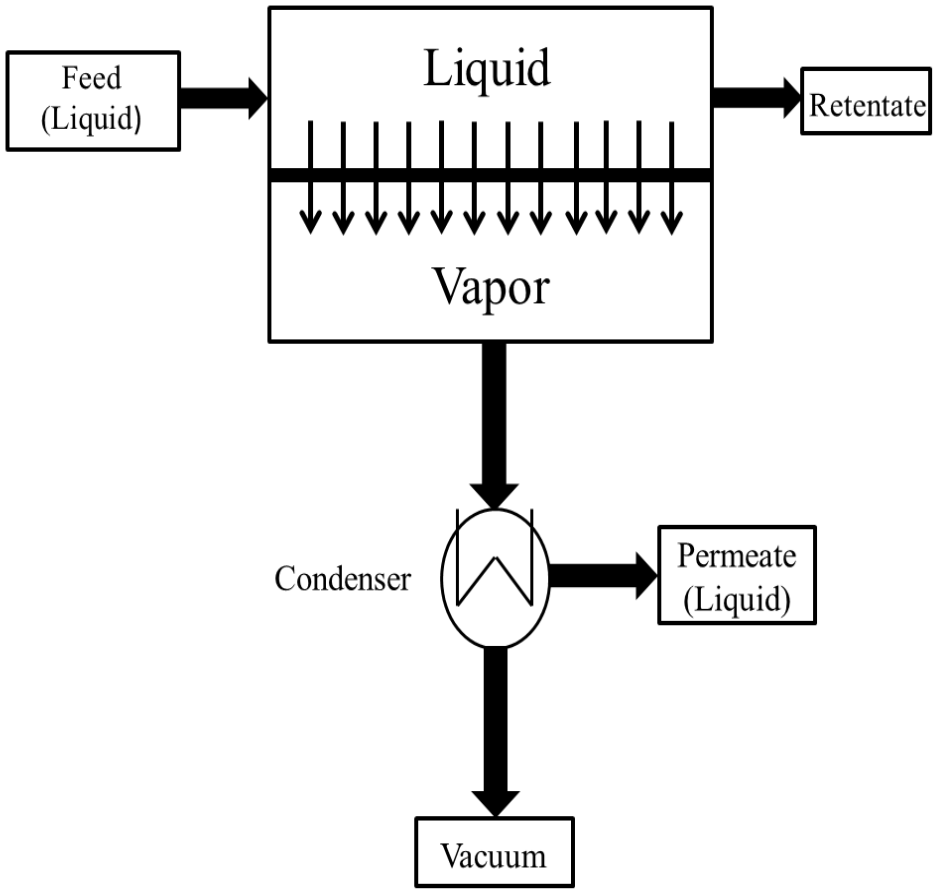

Figure 2.1 Schematic diagram of vacuum pervaporation [Won, 2002]

Pervaporation is advantageous for separating minor components from liquid mixtures. Thus, organophilic membranes are usually used for the removal or recovery of organic compounds from aqueous solutions, and hydrophilic membranes are used for dehydration of organic solvents. The applications of pervaporation can be divided into three types:

1. Removal of organic compounds from aqueous solutions
2. Organic solvent dehydration
3. Organic-organic separation of organic mixtures

Currently, pervaporation has been applied for:

a. Breaking of azeotropes (e.g. ethanol/water, isopropanol/water)
b. Removal of organic solvents from industrial wastewater
c. Enrichment of organic compounds from aqueous solutions

There are also some other applications of pervaporation in the food processing such as aroma recovery [Catarino et al., 2009; Shepherd et al., 2002]. The development of pervaporation for the separation of organic mixtures is still quite limited since the membrane stability remains an issue under harsh chemical conditions.

Separation by pervaporation is based on the selective permeation of certain components in a liquid mixture. The mass transport can be described as a three-step process: (a) sorption, (b) diffusion, and (c) desorption. Step (a) and (b) are the steps that determine which component permeates through the membrane preferably. In other words, the selectivity depends on the physical-chemical interactions between the membrane material and the permeants, and it is not determined by the relative volatility as in distillation. Therefore, the ability to separate azeotropes or close-boiling mixtures by pervaporation is unique characteristics of pervaporation. Table 2.1 shows some studies on pervaporation separation over the past few years.

Unlike distillation where latent heat is need to evaporize the liquid, pervaporation only needs to vaporize the permeated species at any operating temperatures. The energy required in pervaporation is equal to the heat of vaporization of the permeated species from a thermodynamic point of view. This drastically reduces the energy consumption in comparison to distillation process. For example, using pervaporation for separating ethanol from ethyl tert-butyl ether (ETBE) could save up to 60% on operating costs in comparison to distillation process [Streicher et al. 1995]

In pervaporation, the upstream side of the membrane is at ambient pressure, and the

downstream side is under vacuum. This allows the certain components to permeate through the membrane and get collected at the downstream side as vapor. The driving force for the mass transfer through the membrane depends on the chemical potential gradient across the membrane, which is not limited by the osmotic pressure as in reverse osmosis. For example, pervaporation can concentrate ethanol from 85 to more than 99 wt% in an aqueous solution, while an extremely high operating pressure would be needed to overcome the osmotic pressure if reverse osmosis is used [Feng and Huang, 1997]. In addition, both the separation factor and permeation flux in pervaporation are generally higher than in reverse osmosis under the same operating conditions [Choudhury et al., 1985]. Pervaporation involves a phase change of the permeate from liquid to vapor, and thus, energy is used to pressurize the feed liquid, operate vacuum pump and evaporize the permeate. However, this energy consumption is much lower than reverse osmosis operation. Normally, thermal energy used for permeate evaporation can be supplied by heating the feed liquid or by a sweeping gas on the permeate side, or even direct heating of the membrane [Wnuk and Chmie, 1992].

Pervaporation plants can be in either large or small scales. It is easy to integrate pervaporation units with other separation units (e.g., distillation) in order to enhance the overall separation efficiency. For example, using a hybrid pervaporation-distillation process in ethanol-production could save 66% of the operating costs in comparison to using distillation process only [Sander and Soukup, 1988].

Table 2.1 Studies on pervaporation process

Feed(liquid mixture)	Membrane	Reference
Water/Ethanol	Aromatic polyetherimide	[Huang and Feng, 1992]
Water/ethylene glycol	Chitosan/polysulfone composite membrane	[Feng and Huang, 1996a]
Acetone-butanol-ethanol (ABE)	Polydimethylsiloxane	[Kawedia et al., 2000]
Diemthyl carbonate/methanol	Poly(acrylic acid)/poly(vinyl alcohol) blend membranes	[Wang et al., 2007]
n-butanol/ aqueous solution	Silicalite-filled poly(dimethyl siloxane) membrane	[Fouad and Feng, 2009]
Water/ ethylene glycol	Polymerized polyamide membrane	[Xu et al., 2010]
Water/isopropanol	Hydrophilic chitosan-modified polybenzoimidazole membrane	[Han et al., 2014]
Water/ethylene glycol	Polyamide and polydopamine composite membranes	[Wu etal., 2015]
Water/ethanol	Boron-substituted silicalite-2 membranes	[Chai et al., 2015]
Water/butyric acid	Poly(ether block amides) composite membranes	[Choudhari et al., 2015]
toluene/*n*-heptane	Tubular composite membrane by self-crosslinkable hyperbranched polymers	[Wang et al., 2015]
Water/acetic acid	Polyphenylsulfone-based membranes, modified with silica nanoparticles	[Jullok et al., 2016]

2.2 Mass transport mechanism

2.2.1 Solution-diffusion model

There are several models to describe mass transport in pervaporation [Shieh and Huang, 1998; Okada and Matsuura, 1991; Kedem, 1989], among which, the solution-diffusion model is the most popular one. According to the solution-diffusion model, the mass transfer in pervaporation can be divided into three steps, as shown in Figure 2.2,

1. Sorption of the components from the feed into the membrane;
2. Diffusion of the adsorbed components through the membrane;
3. Desorption of the permeating components from the other side of the membrane as vapor.

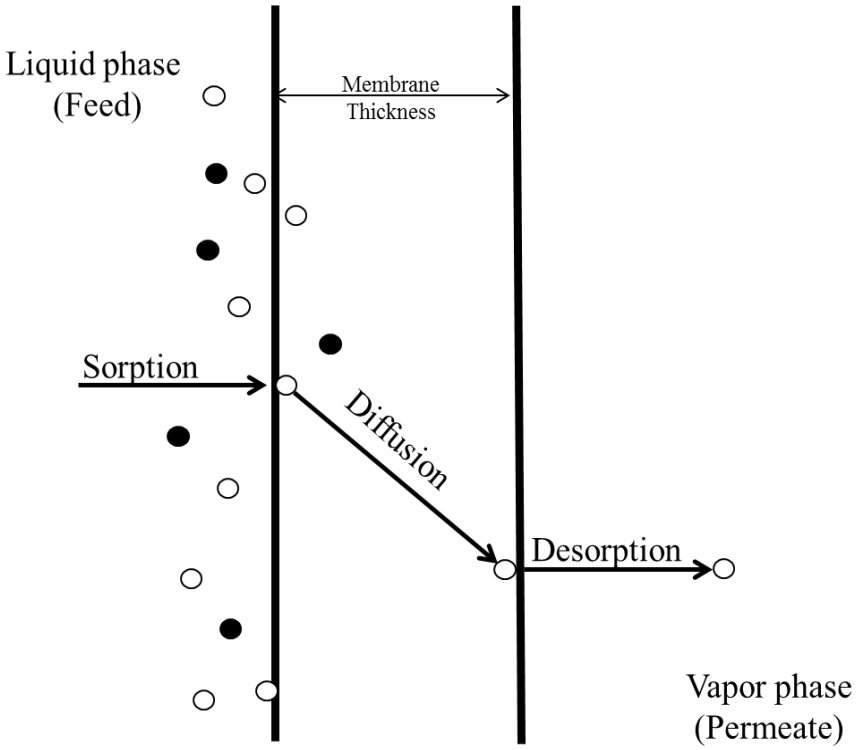

Figure 2.2 Illustration of solution-diffusion model for mass transport in pervaporation [Won, 2002]

In the solution-diffusion model, the components which need to be transported must be first dissolved into the membrane, and this step is may be a selective step if the components to be separated have different solubilities in the membrane. The diffusion step is the rate-controlling step. The permeability of a component in the membrane is determined by the diffusion coefficient and solubility coefficient [Feng and Huang, 1996b]. The desorption step is commonly considered to be fast enough that it has little impact on the pervaporation transport. In addition, the pressure of the permeate side is maintained lower than the saturated vapor pressure of the feed solution to induce mass transport in the membrane. Therefore, the pervaporation is mainly controlled by the sorption and diffusion.

Base on the solution-diffusion model, if both solubility and diffusivity coefficients are constant, the flux equation can be expressed by [Feng and Huang, 1996a]:

$$J_i = (\frac{P_i}{l})(X_i\gamma_i p_i^{sat} - Y_i p^p) \tag{2.1}$$

where l is the membrane thickness, p_i^{sat} is the saturated vapor pressure of component i, γ_i is the activity coefficient of the permeant in liquid feed, and p^p is the permeate pressure. J_i is the permeation flux, which is the permeation rate per unit membrane area:

$$J_i = N_i/A \tag{2.2}$$

In Equation (2.1), the quantity (P_i/l) is called the permeance of the membrane, which is the membrane permeability normalized by membrane thickness. It is equal to the permeation flux normalized by the transmembrane driving force expressed by the pressure difference$(X_i\gamma_i p_i^{sat} - Y_i p^p)$.

The permeability in pervaporation process can be expressed as [Feng and Huang, 1996a]:

$$P_i = D_i \cdot S_i \tag{2.3}$$

where P_i is the permeability coefficient, D_i is the diffusivity coefficient and S_i is the

solubility coefficient.

In pervaporation, the effect of operating temperature on permeation flux can be described by an Arrhenius type of equation:

$$J_i = J_{0i}\exp(-\frac{E_{Ji}}{RT}) \tag{2.4}$$

where E_J is as the activation energy for permeation, J_0 is a pre-exponential factor, R is the gas constant, and T is the absolute temperature.

It should be pointed out that Eq. (2.4) has been widely used in pervaporation to calculate the activation energy of permeation from the plot of lnJ vs. $1/\mathrm{T}$. However, the activity coefficient γ_i and the saturated vapor pressure p_i^{sat} are also affected by temperature in different ways, so that E_J is only a rough characterization of the activation energy of permeation.

The temperature dependence of D_i and S_i is commonly described as:

$$D_i = D_0\exp(-E_D/RT) \tag{2.5}$$

$$S_i = S_0\exp(-\Delta H/RT) \tag{2.6}$$

Therefore, the permeability coefficient P_i can be expressed as:

$$P_i = P_0\exp(-E_P/RT) \tag{2.7}$$

where $E_P = (E_D + \Delta H)$ is the activation energy of permeation based on permeability. It combines the activation energy of diffusion E_D and the enthalpy change of dissolution ΔH of the permeant in the membrane; P_0 is a pre-exponential factor which is equal to D_0 multiply S_0. From Equations (2.1) and (2.7)

$$\frac{P_i}{l} = J_i/(X_i\gamma_i p_i^{sat} - Y_i p^p) = (P_{0i}/l)\exp(-E_{Pi}/RT) \tag{2.8}$$

Thus, the activation energy E_P could be evaluated from the slope of the plot $\ln(J/\Delta P)$ vs. $1/\mathrm{T}$. Comparing to saturated vapor pressure p_i^{sat}, the permeate pressure p^p is generally low in pervaporation processes, which can be ignored. Therefore, if the saturated vapor pressure p_i^{sat}

of the feed liquid follows the Clausius-Clapeyron equation and the temperature dependence of activity coefficient of the permeant is unimportant, then the activation energy E_P can be estimated as [Feng and Huang, 1996a]:

$$E_P = E_J - \Delta H_V \tag{2.9}$$

where ΔH_V is the heat of vaporization of the permeant. Evaluating E_J from lnJ vs. $1/\mathrm{T}$ is much easier than evaluating E_P from $\ln(J/\Delta P)$ vs. $1/\mathrm{T}$ data, especially when the permeate pressure is sufficiently low, and the Eq. (2.9) can be used to estimate E_P from the corresponding data of E_J. This equation also explicitly shows the influence of enthalpy change due to the phase change in pervaporation on the permeation. Note that E_P is the activation energy based on permeance that measures the permeability of the membrane, excluding the effect of temperature on the driving force for permeation (i.e., ΔP).

2.2.2 Pore-flow model

Okada and Matsuura [1991] proposed Pore-Flow model to explain the mass transfer in the membrane.

In pore-flow model, it is assumed that there are straight and cylindrical pores with length δ penetrating across the active surface layer of the membrane and all the pores are in an isothermal condition. Figure 2.3 shows a schematic diagram of the pore-flow model.

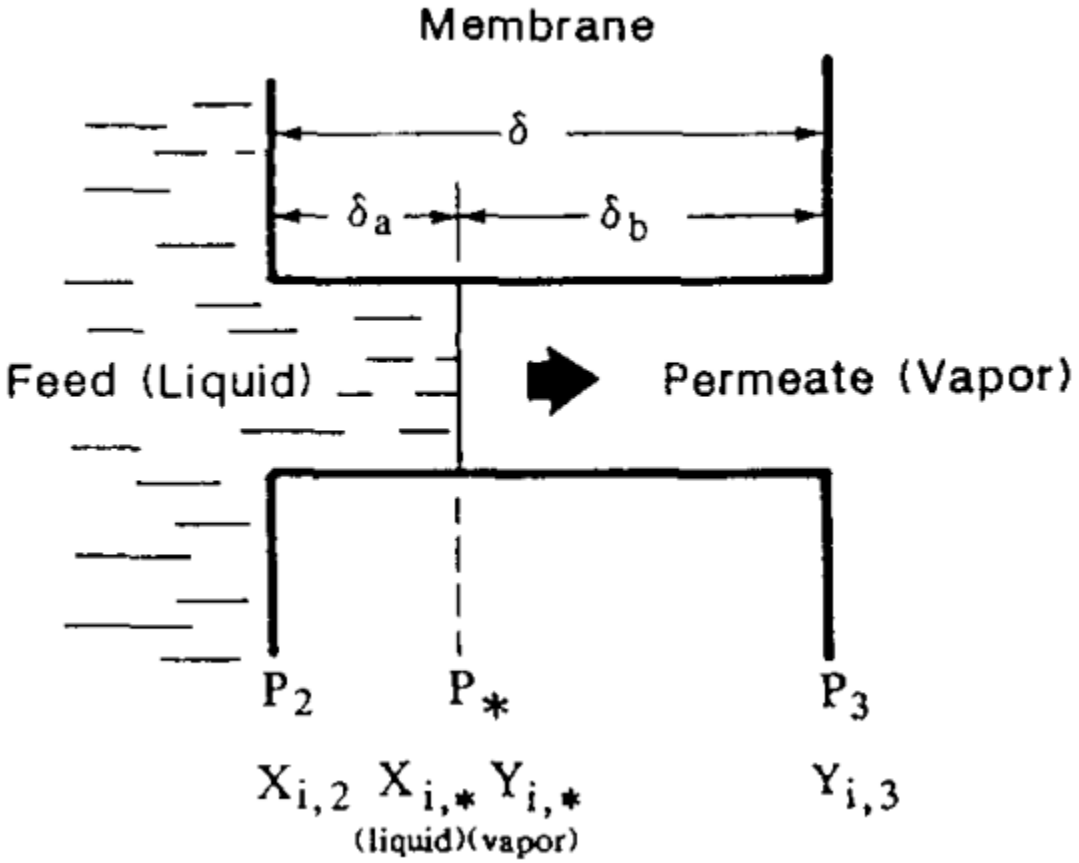

Figure 2.3 Schematic diagram of pore-flow model [Okada and Matsuura, 1991].

The mass transport is divided into three steps:

1. Liquid from the pore inlet transports to the liquid-vapor boundary with a distance δ_a.
2. Evaporation takes place at the boundary of the liquid-vapor phase.
3. Vapor transports to the pore outlet from the vapor phase with a distance δ_b.

In the pore-flow model, the phase change is considered to occur in the membrane, which is the main difference with the solution-diffusion model. Moreover, the phase change of the liquid happens in a certain distance between the membrane surface to the liquid-vapor boundary, where the transport mechanism also changes. Therefore, the transport in pore-flow model can be

considered as a combination of liquid and vapor transport in small pores.

2.3 Membrane performance

In pervaporation separation, three parameters need to be addressed: membrane productivity, membrane selectivity and membrane stability.

Membrane productivity measures the amount of components that permeates through a given area of the membrane in a certain period of time. Membrane productivity is characterized by permeation flux (J),

$$J = \frac{M}{At} \tag{2.10}$$

where M is the total mass of permeate, A is the effective area of the membrane and t is the time. The permeation flux also depends on the intrinsic permeability and the effective thickness of the membrane. Therefore, choosing materials with porper intrinsic permeability or using technological methods to reduce the thickness of the membrane is an effective approach to enhancing the productivity of the membrane.

Membrane selectivity of pervaporative desalination may be characterized by salt rejection (R):

$$R = \frac{C_f - C_p}{C_f} \times 100\% \tag{2.11}$$

where C_f and C_p are the salt concentrations in the feed solution and the permeate solution, respectively.

Membrane stability is also an important factor of the membrane. Under specific system conditions, membrane stability will determine how long both the permeability and selectivity will last in separation process. Membrane stability is affected by thermal, chemical or

mechanical causes. Maintaining the membrane stability is a pre-requirement to achieve good productivity and selectivity.

2.4 Polymer materials for pervaporation membranes

Polymeric materials are widely used for the preparation of pervaporation membranes. They can be divided into three types: glassy polymers, ionic polymers and rubbery polymers [Feng and Huang 1997]. As mentioned before, besides the chemical stability and mechanical properties, high selectivity and permeability are important factors that should be considered when choosing polymers for making.

The characteristics of pervaporation membranes are determined by physical properties and chemical structures of the membranes, as well as the interactions between the permeant and the membrane materials. Methods for the selection of pervaporation membrane materials include [Feng and Huang 1997]:

1. Surface Thermodynamics Approach
2. Contact Angle Approach
3. Liquid Chromatography Approach
4. Polarity Parameter Approach
5. Solubility Parameter Approach

For water desalination, hydrophilic polymers are the most suitable membrane materials. Table 2.2 shows some studies on desalination. Interestingly, there is little published work on the use of elastomeric hydrophilic membranes, such as Pebax®, in pervaporation for water desalination.

Table 2.2 Desalination by pervaporation process

Membranes	Salt	Salt concentration (wt%)	Reference
Sulfonated polyethylene membranes	NaCl	0-176 (g/L)	[Korin et al., 1996]
PEA/PA/PE composite membranes	Untreated seawater and waste water	100g/l of total solids in feed solutions	[Zwijnenberg et al., 2005]
Hydroxyl sodalite membranes	Seawater/ Aqueous solutions of NaCl and $NaNO_3$	Na^+: 8670 (mg/L) in seawater NaCl solutions (0-35 wt%) $NaNO_3$ solutions (0-35 wt%)	[Khajavi et al., 2010]
PVA/MA/silica hybrid membrane	NaCl	_	[Xie et al., 2011]
Tubular MFI zeolite membranes	NaCl	Correspongding to brackish water (0.3-1 wt%) seawater (3.5 wt%) brine water (7.5-15 wt%)	[Drobek et al., 2012]
Natural zeolite clinoptilolite-phosphate composite membranes	Na^+	1310 (ppm)	[An et al., 2014]
Cellulose triacetate membranes	NaCl	100 (g/L)	[Huth et al., 2014]
Cellulose acetate membranes	NaCl	40-140 (g/L)	[Naim et al., 2015]
Carbon template silica membranes	NaCl	40 (g/L)	[Singh et al., 2015]
Graphene oxide/polyacrylonitrile membranes	NaCl	35 (g/L)	[Liang et al., 2015]

2.4.1 Poly(ether-block amide)

Pebax is a family of high-tech copolymer developed by Arkema 25 years ago. The first generation of Pebax® polymers was poly(tetramethylene oxide) (PTMO) based. Poly(ethylene oxide) (PEO) was used instead of PTMO for the second generation of Pebax polymers [Jonquières et al., 2002]. Until now, Pebax® has become a good choice for many applications.

Pebax® (polyether block amide) (PEBA) is a family of block copolymers, and they are thermoplastic elastomers without plasticizers, combining rigid polyamide (PA) segments and flexible polyether (PE) segments. Fig2.4 shows the general structure of Pebax®.

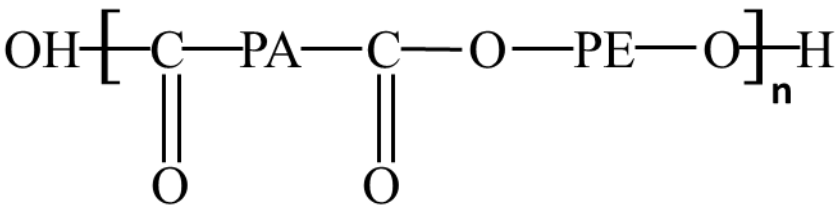

Figure 2.4 general structure of Pebax [Bondar et al. 1999]

where PA is a "hard" block consisting of aliphatic polyamide (i.e. PA6, poly[imino(1-oxodo-decamethylene)]), and PE is a "soft" block consisting of polyether (i.e. PEO, poly(ethylene oxide). The hard PA blocks provide mechanical stability to the membrane and the soft PEO blocks support high permeability due to the flexibility of the ether linkages.

Pebax polymers combine the properties of hardness, good elasticity and easy processing, which makes them a ideal material in many applications. Due to its outstanding thermal resistance, Pebax polymers showed excellent dynamic performance from -40℃ to +80℃.

Moreover, Pebax® has corrosion resistance to most chemicals, and anti-oxidantion properties.

Pebax polymer was used in this study. It was a hydrophilic block copolymer consisting of 55 wt% PEO and 45 wt% PA [Bondar et al. 1999]. Some selective properties are listed in Table 2.3.

Table 2.3 Specialty Pebax® polymer

Property	Typical Value
PE Content (wt%)	55
Density[a] (g/cm^3)	1.07
X_c Crystallinity in PA Block[a] (wt%)	40
T_g[b] (℃)	-55
T_m (PE)[b] (℃)	11
T_m (PA)[b] (℃)	156
Melting Point[a] (℃)	158
Water Absorption at Equilibrium[b] (%)	1.4
Hardness[b] (Shore D)	40
Tensile Test, Stress at Break[b] (MPa)	30

[a] Pebax® MV 1074 SA 01
[b] Bondar et al. (1999)

Pebax has been utilized for gas separation due to its good selectivity to carbon dioxide (CO_2) [Bondar et al. 1999]. However, there is little information about its potential use in pervaporation. Table 2.4 shows the water vapor flux of the membranes made of different grades of Pebax polymers [Nguyen et al, 2001]. Pebax® 1074 shows the best water vapor permeability compared to other Pebax® grades.

Table 2.4 Water vapor permeation rate of different Pebax films[a]

Pebax® grade	Water flux (kg/m^2/day)
3533	5.9
1041	28.8
3000	67.0
1074	85

[a] At specific operating conditions (38℃, membrane thickness 25μm)

2.5 Desalination technologies

Desalination is a process that removes salts from seawater or brackish water. Saline water is desalinated to produce water suitable for irrigation or human consumption. Desalination is used in many submarines and ships for supply of fresh water. Many researchers focused on developing cost-effective desalination methods to provide water for human use.

Due to energy consumption, the costs of desalinating sea water are generally higher than other water treatment (e.g. groundwater, rivers or industrial wastewater). However, the crisis of water shortage is one of the most serious issues in the world. Presently, over one-third of the population on the earth live in water-stressed countries, and this number is predicted to rise to nearly two-thirds by 2025. Thus the desalination industry for water treatment is important to meet the societal needs.

Desalination technology is quickly expanding around the world, especially in water-shortage countries. In Australia, over 150 sea water reverse osmosis plants ranging in size from 100 to 444,000 m^3/day are either in operation or under construction [Global Water Intelligence]. According to the International Desalination Association, 15,988 desalination plants are operated worldwide in June 2011, producing 66.5×10^6 m^3/day for 300 million people [Henthorne, 2012]. This number has been updated to 78.4 $\times10^6$ m^3/day in 2013 [Global Water

Intelligence]. The single largest desalination project is Ras Al-Khair in Saudi Arabia, which produced 1.025×10^6 m^3/day cubic 2014 [Global Water Intelligence].

Recently, many desalination methods are used worldwide. Figure 2.5 shows the main technologies that have been used in practice. The most widely used operations are multi-stage flash distillation and reverse osmosis.

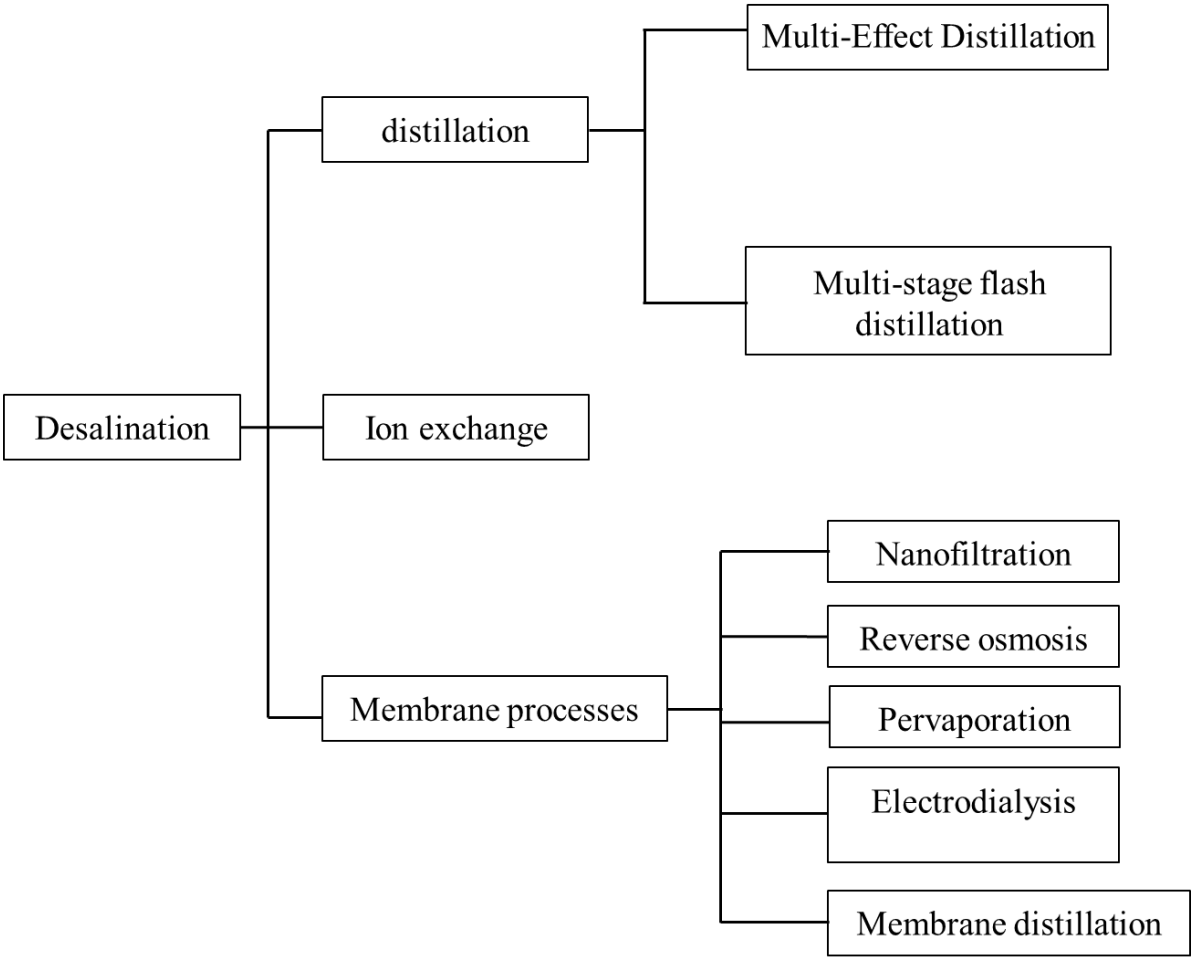

Figure 2.5 Classification of seawater desalination methods

Distillation is a process of separating the salts from seawater by selective evaporation and condensation. It is the oldest desalination technology; a simple distiller was installed on the boat in order to provide plenty of fresh water when people sailing on the sea. Base on this principle,

distillation process has been improved in many aspects in order to reduce the cost of desalination, and this led to multi-stage flash distillation, multiple-effect distillation, vapor-compression and membrane distillation [Alkhudhiri et al., 2012].

Figure 2.6 shows the principle of multi-stage flash. Each stage includes a condensate collector and a heat exchanger. The sea water is heated to a certain temperature and then sent to the heat exchanger, which is maintained at vacuum conditions to induce vaporization of seawater in the heat exchanger. Finally, the vapor condenses to liquid as fresh water for use.

MSF distillation plants, especially large scale units, are often paired with power stations. Waste heat from the power stations can be used to heat the seawater. Meanwhile, this process also supports the cooling for the power stations. This integrated operation will decrease the energy costs by 50-67%. Therefore, MSF is a popular desalination process. For example, the Saline Water Conversion Corporation of Saudi Arabia is currently producing over 16% of the total worldwide desalted water [Wangnick, 1998], and multi-stage flash (MSF) distillation accounts for 94% of its total desalinated water.

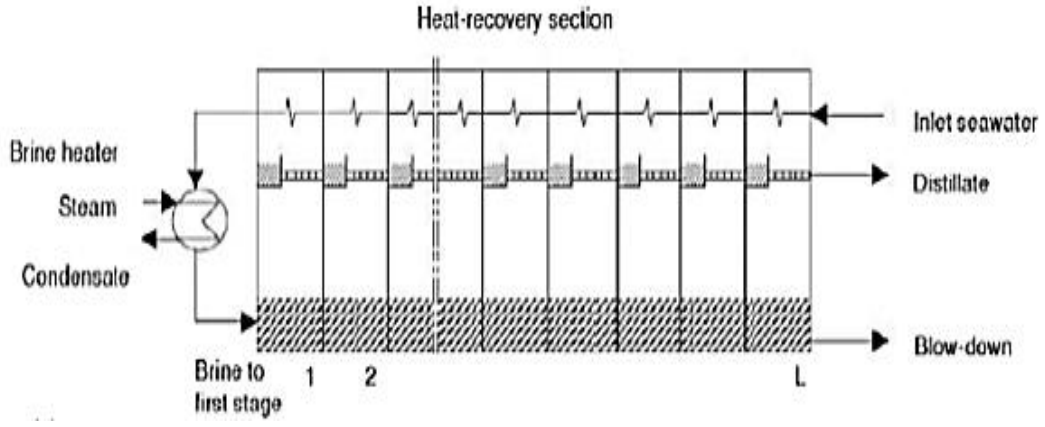

Figure 2.6 Multi-stage flash plants [Al-Rawajfeh, 2016]

Membrane distillation (MD) is a thermally driven membrane separation process. The liquid

(e.g., seawater) contacts a microporous hydrophobic membrane, and only water vapor molecules pass through the membrane. The driving force of MD process is given by the vapor pressure difference, which is commonly caused by a temperature difference. MD process can be used in wastewater treatment, desalination and food processing. There are four MD configurations that have been used to separate aqueous feed solutions [Alkhudhiri et al., 2012]:

1. Direct Contact Membrane Distillation (DCMD)
2. Vacuum Membrane Distillation (VMD)
3. Air Gap Membrane Distillation (AGMD)
4. Sweeping Gas Membrane Distillation (SGMD)

Vacuum membrane distillation (VMD) generally has a high permeation flux compared to other configurations. In addition, the heat lost by conduction is negligible, which is a significant advantage [Lawson and Lloyd, 1997]. Figure 2.7 shows a schematic diagram of VMD. Moreover, in MD, the membrane used should have a low thermal conductivity to minimize heat loss. It should also have a low resistance to water vapor transport. The polymers commonly used for MD membrane are polypropylene (PP), polytetrafluoroethylene (PTFE) and poly(vinylidene fluoride) (PVDF).

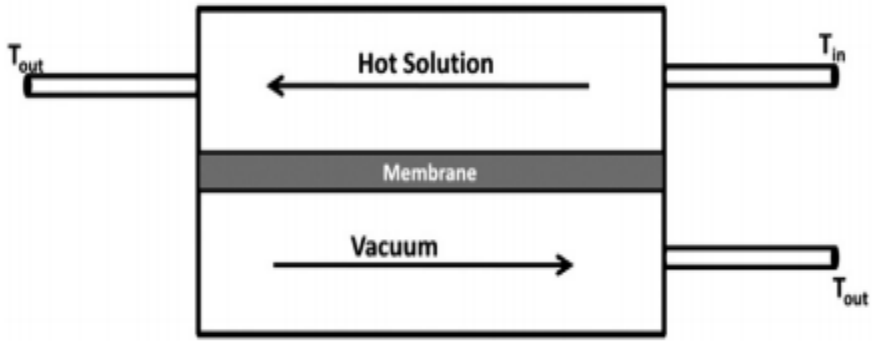

Figure 2.7 Vacuum membrane distillation (VMD) [Alkhudhiri et al., 2012]

Osmosis has been known for centuries. Think that a semipermeable membrane divides a container into two parts, which were filled with pure water and seawater, respectively. After a period of time, the level of sea water will rise and that of pure water will decline, because the water molecules from pure water side transport through the semipermeable membrane to the sea water side. This phenomenon is called osmosis. However, if an external pressure high enough is applied to overcome the osmotic pressure, then the water molecules from seawater side will transport through the membrane to the pure water side. This process is called Reverse Osmosis (RO). Figure 2.8 shows the schematic diagram of reverse osmosis.

The most common application of reverse osmosis is the separation of fresh water from seawater. Most commercially available RO membranes are thin film composite membranes comprsing of an aromatic polyamide active layer (~50-250 nm), an asymmetric polysulfone support (~50 μm-thick), and a nonwoven polyester fabric backing (~150 μm-thick) [Petersen, 1993]. The polyamide active layer is considered to be dense, which allows only water molecules to pass through and prevents the solutes, such as salt ions. This process requires a high pressure on the high concentration side of the membrane, usually 2-17 bar for brackish water and 40-70 bar for seawater [Rao, 2011]. Reverse Osmosis is best known for its application in desalination of seawtaer. It has been also used to purify water for domestic, medical and industrial applications more recently.

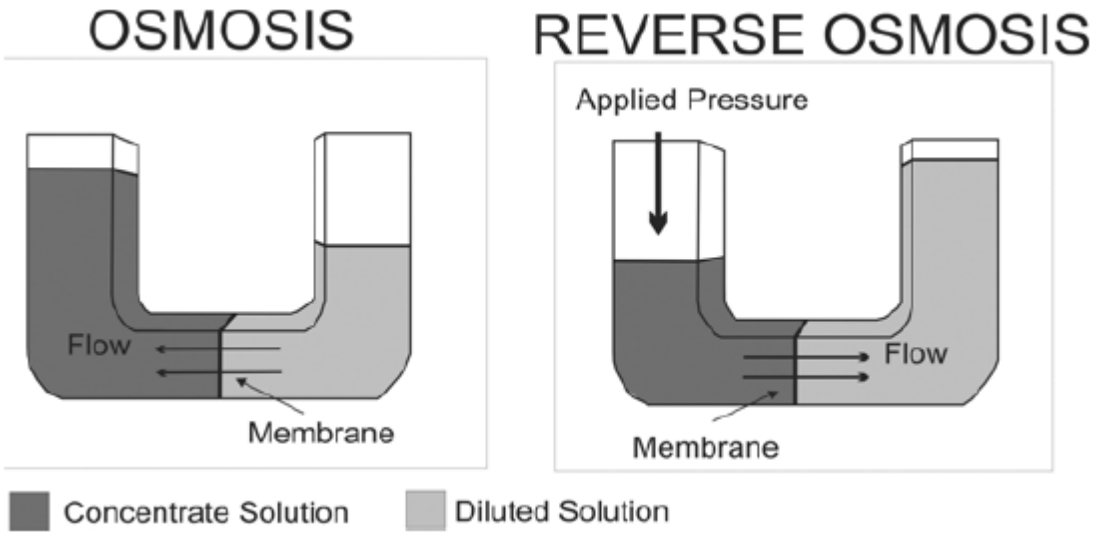

Figure 2.8 Reverse osmosis principle. Left: osmosis; right: reverse Osmosis [Fritzmann et al., 2007]

This study will focus on pervaporative desalination of high salinity water for which the convential reverse osmosis is no longer effective because of the very high osmotic pressure involved.

Chapter 3

Experimental

3.1 Membrane preparation

The Pebax polymer was supplied by Arkema Inc.. Homogeneous membranes were prepared using the solution-casting method. Firstly, 18 wt% of Pebax polymer was dissolved in N-methyl-2-pyrrolidone (NMP), (Acros Organic Inc.). The polymer-NMP mixture was stirred for 24 h at a constant temperature of 100℃. Then the homogeneous polymer solution was allowed to stand at 100℃ for 12 h for degassing. The hot polymer solution was finally cast on a preheated glass plate (90℃) at a controlled membrane thickness. The solvent in the cast membrane was evaporated in an oven at 90℃ for 12 h, and then the glass plate together with the membrane was immersed into water to take off the membrane from the glass plate. The membranes were stored in a vacuum oven at ambient temperature. Membranes with five different thicknesses (i.e. 39, 48, 56, 71, and 88μm) were prepared.

3.2 Pervaporative desalination

The experimental setup for pervaporative desalination is shown in Figure 3.1. The membrane was mounted in the membrane cell, and it had an effective membrane area of 22.05 cm^2. The feed solution was continuously supplied to the upstream side of the membrane surface using a circulation pump. The temperature of the feed solution was controlled by a thermoregulator and a heating mantle. The driving force for permeation was provided by a vacuum pump, and the permeated water vapor was collected in a cold trap immersed in liquid

nitrogen (around -195℃). The compositions of the feed and permeate were determined using a conductivity meter (WTW inoLab Cond Level 2).

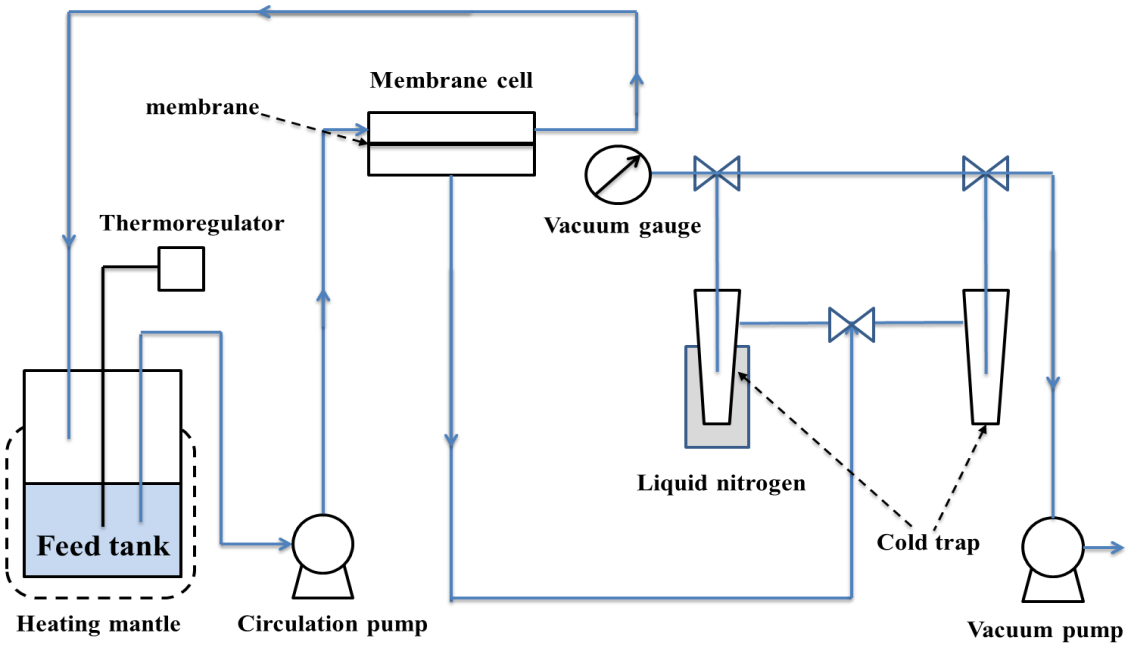

Figure 3.1 Schematic diagram of experimental setup for pervaporative desalination

The membrane was first tested with pure water pervaporation for 3 h to reach a steady state. Before each pervaporation run, the feed solution was circulated for 1 h to condition the membrane. The membrane was washed with de-ionized water for 10 min to remove any salt residues after each pervaporation run. The permeation flux of water (J) was determined from the amount of permeate water collected over a given time interval,

$$J = \frac{M}{At} \tag{3.1}$$

where M is the total mass of permeate water, A is the effective area of the membrane and t is the time. Membrane selectivity of pervaporative desalination may be characterized by salt rejection (R):

$$R = \frac{C_f - C_p}{C_f} \times 100\% \quad (3.2)$$

where C_f and C_p are the salt concentrations in the feed solution and the permeate solution, respectively.

The pervaporative desalination experiments were repeated at least three times and the overage data were presented. The experimental errors of flux and salt rejection were within 2% and 0.01%, respectively.

3.3 Sorption/desorption experiments

The sorption and desorption experiments were carried out to investigate solubility of water and salt in the membrane. The dried membranes were immersed into the aqueous solutions of various salts at different concentrations at temperature (25℃). The concentration of the solutions were set at 1, 5, 10, 15, and 20 wt%, respectively. The membrane samples were submerged in these solutions for 24 h to reach the sorption equilibrium. The sorption uptake in the membrane was calculated from:

$$m_1 = m_2 - m_0 \quad (3.3)$$

where m_0 and m_2 are the weights of the membrane sample before and after sorption, respectively, and m_1 is the total weight of water and salt sorbed into the membrane.

In order to calculated the respective weight of water and salt in membrane, the membrane sample after the sorption was placed in a vacuum oven at 60℃ for 24 h to achieve a complete desorption of water from the membrane. Thus, the sorption uptake of water can be calculated as:

$$m_w = m_2 - m_3 \quad (3.4)$$

where m_w is the weight of water sorbed in the membrane, m_3 is the weight of the dry membrane sample after water desorption. Then, the sorption uptake of salt can be expressed as:

$$m_s = m_3 - m_0 \quad (3.5)$$

where m_s is the weight of the salt sorbed in the membrane. The mass uptake of water and salt can be readily converted to molar uptake using their molar weights.

The membrane thickness was around 56 μm in this sorption and desorption experiments, and each experiment was repeat at least twice.

3.4 Diffusion/permeation experiments

The diffusivity and permeability of salts in the membrane were investigated by permeation experiment. Figure 3.2 shows the experimental apparatus, which is composed by a source compartment of 100 ml capacity and a receiving compartment of 1500 ml capacity. The membrane was fixed at the bottom of the source compartment and suspended on the top of the receiving compartment. Stirrers were equiped in both source and receiving compartments to eliminate the boundary layer effect. The receiving compartment was filled with 950 ml of deionized water before the experiment started. Then, the source compartment was filled with 50 ml of salt solution at a certain concentration (i.e., 1, 5, 10, 15, and 20 wt%) to induce diffusion and permeation through the membrane. The membrane thickness used in this study was the same as that used in the sorption/desorption experiments (i.e., 56 μm), and the effective membrane area for permeation was 11.34 cm^2. The experiment was carried out at 25℃.

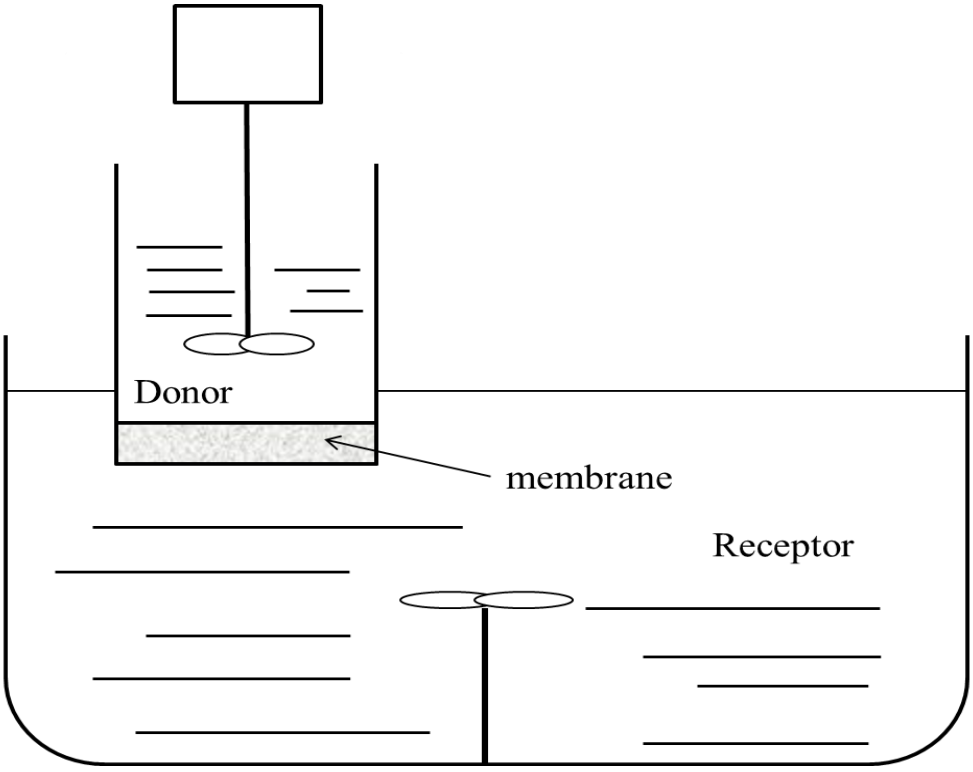

Figure 3.2 Schematic diagram of diffusion/permeation experiments [Chen et al., 2010].

Fig. 3.3 is a schematic diagram showing the three stages during the diffusion through a membrane: (1) an initial stage of transient permeation, (2) quasi-steady-state when the concentration difference through the membrane is nearly constant, and then (3) unsteady state permeation when the concentration at the receptor side becomes considerably high. During the initial period of diffusion, there is a time lag (θ) in the permeation. The diffusivity coefficient can be in principle determined from the time lag [Chen et al., 2010]. The long time ($>3\theta$) permeation can be considered to have reached quasi-steady state, and thus the permeability coefficient can then determine from the slope of the long time permeation curve.

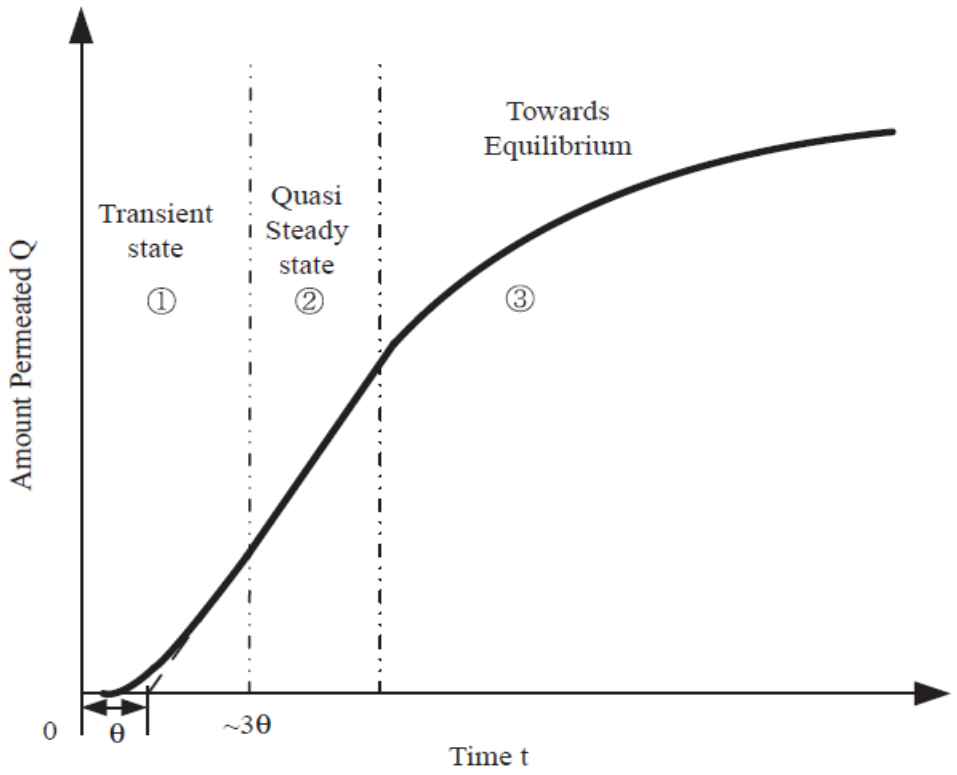

Figure 3.3 Quantity of permeant diffused to the receptor of the membrane [Chen et al., 2010].

The permeability coefficient P and diffusion coefficient D were determined by an approach combing time lag and mass balance methods. As shown in Figure 3.4, this approach involves two steps: (1) determine the upper limit of time beyond which the concentration variation is no longer due to the transient permeation, and thus the diffusion coefficient D was determined from the short-time permeation data. (2) Based the time-lag (θ) obtained, the impact of transient permeation could be neglected after three times of the time-lag, and thus the long time ($t>3\theta$) permeation data were used for mass balance analysis, and then the permeability coefficient P was determined [Chen et al., 2010]. Additional considerations will be addressed in the results and discussion section.

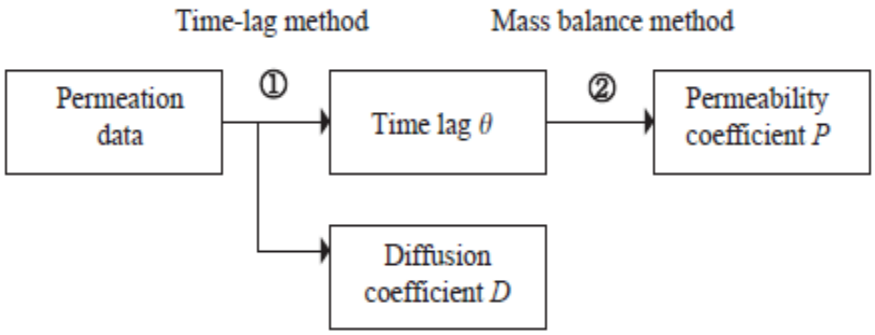

Figure 3.4 Determination of diffusion and permeability coefficients [Chen et al., 2010] .

3.5 Pervaporation with multi-layer membranes to determine concentration profile in the membrane

Concentration profile of salts in the membrane was determined by pervaporative desalination using multi-layer membranes. In this experiment, five sheets of membranes with the same thickness and area (40μm and 22.05 cm^2) were laminated tightly and placed together in the membrane cell. The total membrane thickness was around 200μm. The concentration of feed solution varied from 2 to 20 wt%, and the experiments were operated at temperature of 25℃. After continuous operation for 10 h, these five membrane sheets were immediately separated and put each membrane into 100ml of deionized water separately for 24 h to remove the salt from the membrane. The amount of salt dissolved in the membrane, which was equal to that dissolved in the water, was determined by measuring the salt concentration in water using the conductivity meter. Here, the salt amount sorbed in the membrane was determined from the change in salt concentration in the leached solution rather than the weight variation of the membrane, because the amount of salt was very small and it was hard to be accurately determined from weight

change. This allowed us to determine the concentration profile of salts in the membrane during steady state pervaporation process for water desalination.

Chapter 4

Results and Discussion

In pervaporation, a liquid feed contacts with the membrane, and mass transfer through the membrane takes place under vapor pressure difference between the feed and permeate. Currently, the main industrial application for pervaporation is dehydration of organic mixtures or organic and organic separation [Huang, 1991]. Water desalination by pervaporation is developed recently. Same as other pervaporation applications, the membrane used for pervaporative desalination by pervaporation is also nonporous. The membrane used in this study was made from Pebax polymer which has an outstanding permeability to water vapor [Nguyen et al, 2001]. The membrane performance under various operating conditions was investigated. Moreover, the advantages of desalination by pervaporation compared with other membrane processes (e.g. reverse osmosis and membrane distillation) will be also discussed.

4.1 Effect of operating conditions on membrane performance

4.1.1 Effect of feed concentration

In this part, the effects of feed salt concentration, ranging from 1 to 20 wt%, on water desalination pervaporation performance were investigated. Three salts (i.e., NaCl, Na_2SO_4 and $MgCl_2$) were selected as model solutes in the water desalination study. The membrane thickness was 56μm in this part of the study. Figs. 4.1 to 4.3 show the effects of feed salt concentration on water flux for the aqueous solutions containing these three salts.

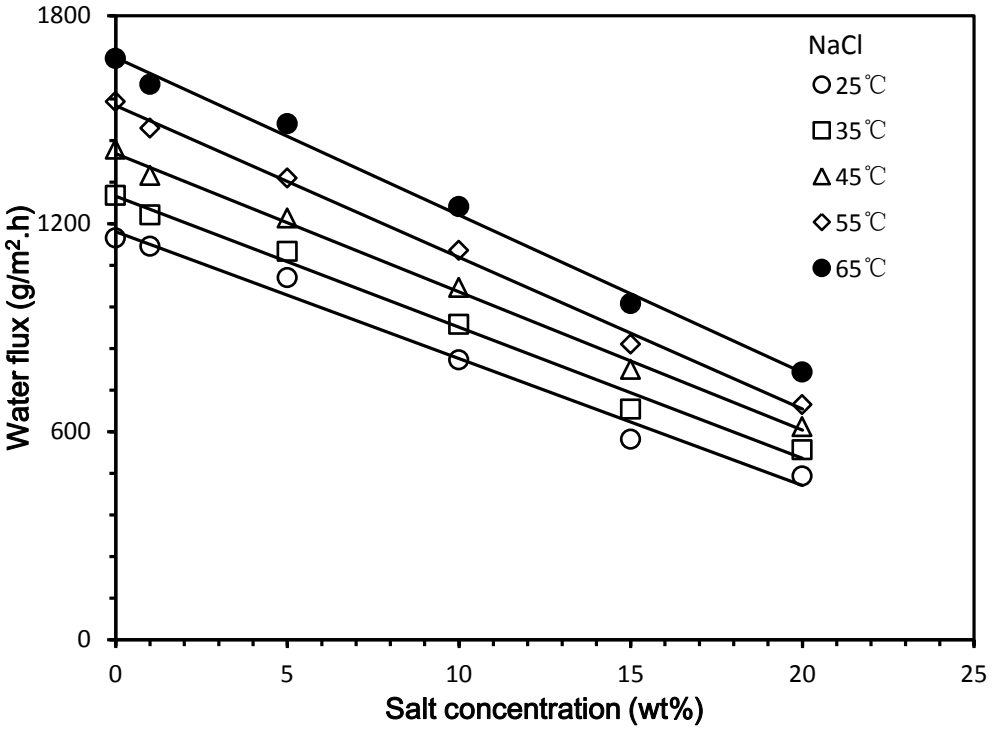

Figure 4.1 Effects of NaCl concentration in feed on water flux. Membrane thickness 56µm.

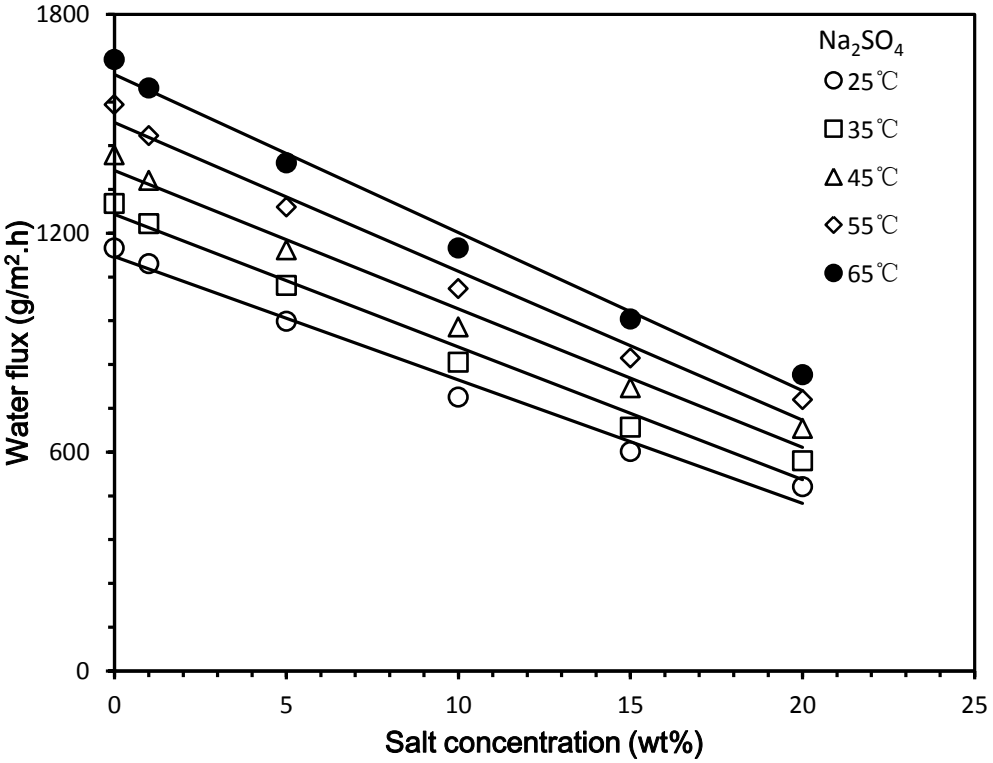

Figure 4.2 Effects of Na_2SO_4 concentration in feed on water flux. Membrane thickness 56µm.

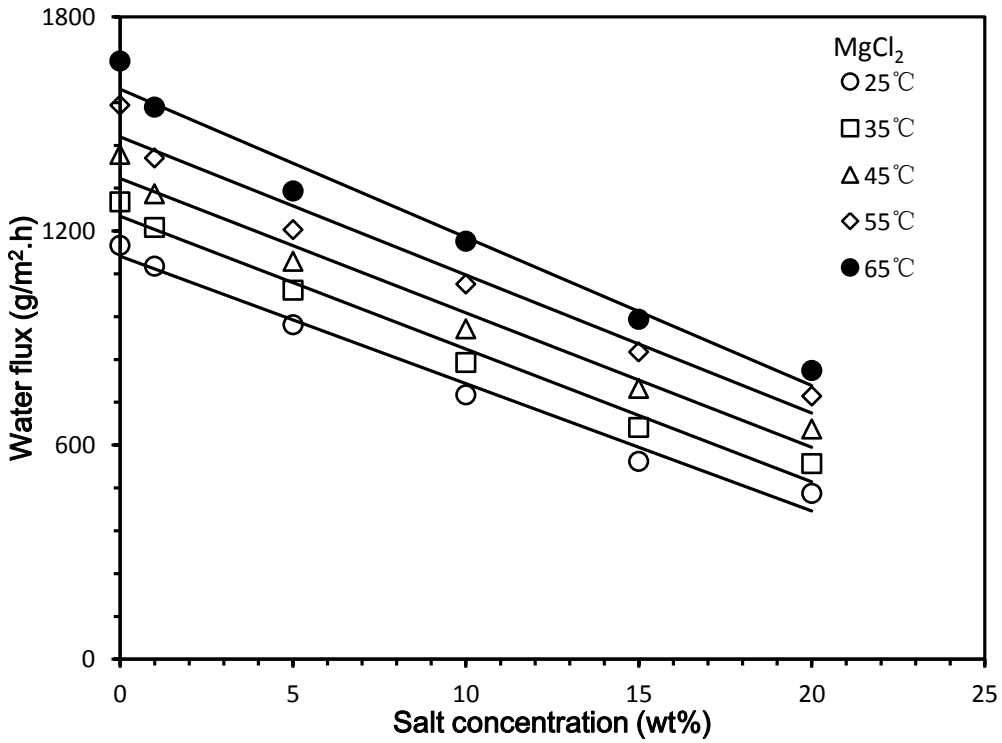

Figure 4.3 Effects of $MgCl_2$ concentration in feed on water flux. Membrane thickness 56μm.

As expected, the water flux decreased with an increase in the salt concentration in the feed solution. When the salt concentration in the feed increases, the saturated vapor pressure of water decreases, resulting in a decline in water permeation flux. However, there is no significant difference in water flux among the different salt solutions (i.e., NaCl, Na_2SO_4 and $MgCl_2$) at a given salt concentration in the solution.

The most popular industrial desalination process is the seawater reverse osmosis. The seawater needs a high operating pressure (60-80 bar) by reverse osmosis desalination and water recovery rate is quite low (25-40%) [Avlonitis et al., 2003]. To reach an overall recovery over 90% would require an operating pressure greater than 120 bar [Chong et al., 2015]. The operating pressure and salt rejection by pervaporation and reverse osmosis were shown in Table 4.1. It can be seen that the pressure difference of pervaporation was maintained approximately as 1 bar by a

vacuum pump in this study, which is much lower than that used in RO (75 to 125 bar). The concentration of feed solution suitable for RO was limited to a certain range since high osmotic pressures need to be overcome for high salinity water. However, in pervaporation, the concentration of salt in the solution can be high as 20 wt%, as shown in Table 4.2, and the salt rejection can still be very high (over 99.9%). From the aspects of energy-consumption and salt rejection, pervaporation is advantageous in desalination, especially for high salinity water. Compared with membranes prepared with other polymers, the membrane used in this study showed a significant higher water permeation flux, even at high feed concentrations (shown in Table 4.3). Therefore, Pebax polymer is a good choice as a membrane material for pervaporative desalination of high salinity water. It may be pointed out that a much higher flux will be obtained if the membrane thickness can be reduced significantly via the use of composite membranes (shown in Table 4.4)

Table 4.1 Comparison of operating conditions by pervaporation and reverse osmosis in desalination

Operation methods	Salt concentration (g/L)	Temperature (℃)	Difference pressure (bar)	Salt Rejection (%)	References
Pervaporation	10	25	~1	>99.9	This study
	10	35	~1	>99.9	
Reverse Osmosis	10	22.5	7.5	66.002	[Khayet et al., 2011]
	10	22.5	12.5	90.681	
	10	37.5	7.5	67.163	
	10	37.5	12.5	90.173	

Salt: NaCl

Table 4.2 A comparison of desalination performance

Process mode	Membrane materials	Salt concentration (NaCl wt %)	Salt rejection (%)	References
Pervaporation	Pebax copolymer	1-20	>99.9	This study
Reverse osmosis	MFI-ZSM-5 (Si/Al=50-65)	0.5	93	[Li et al., 2007]
Reverse osmosis	TM 810	-	99.1	[Pislor et al., 2011]
Membrane distillation	MFI-ZSM-5 (Si/Al=100)	3.8	99	[Duke et al., 2009]
Membrane distillation	Cobalt oxide silica	1-15	99	[Lin et al., 2012]

Table 4.3 A comparison of desalination performance by pervaporation for different homogeneous membranes

Membrane materials	NaCl concentration (g/L)	Temperature (℃)	Water Flux [kg/(m^2.h)]	References
Pebax copolymer	0-200	25-65	0.5-1.7	This study
Poly(ether amide)	35	46-82	0.2	[Zwijnenberg et al., 2005]
Poly(ether ester)	3.2-5.2	22-29	0.15	[Quiñones-Bolaños et al., 2005]
NaA zeolite membrane	35	69	1.6	[Cho et al., 2011]
Polyester	100	50	0.54	[Huth et al., 2014]

Table 4.4 Desalination performance by pervaporation using composite membranes.

Membrane materials	NaCl concentration (g/L)	Temperature (℃)	Membrane thickness (μm)	Water Flux [kg/(m^2.h)]	References
ZSM-5/Silicalite-1	3	75	6	12.5	[Drobek et al., 2012]
Cetyltrimethylammonium bromide-silica membrane	40	20	0.21	2.6	[Singh et al., 2015]
Cellulose diacetate on polytetrafluoroethylene	40	40	3.5	5.1	[Kuznetsov et al., 2007]
Poly(vinyl alcohol) membranes over polysulfone hollow fiber support	30	70	0.1	7.4	[Chaudhri et al., 2015]
Poly(vinyl alcohol)/polyacrylonitile	5	20	0.62	9.04	[Liang et al., 2014]
Poly(vinyl alcohol)/maleic anhydride/silica	2	22	10	6.9	[Xie et al., 2011]
Fluoroalkylsilane-ceramic	30	40	23	5	[Kujawskia et al., 2007]

4.1.2 Effect of temperature

Temperature is an important factor in pervaporation, because it influences the saturated vapor pressure of water in the feed, and the permeability of water in the membrane. Generally, water flux increases with an increase in temperature. According to the Eyring theory of diffusion, an increase in temperature makes the permeant molecules more energetic and easier for diffusive migration [Xu et al., 2010]. In addition, the thermal motion of the polymer chains in the membrane increases. These two factors lead to an increased diffusivity of the penetrant molecules in the membrane [Xu et al., 2010]. On the other hand, an increase in temperature increases the vapor pressure of water in the feed, and thus, increases the driving force for mass transport of water across the membrane [Xu et al., 2010]. Normally, the temperature dependence of water flux follows an Arrhenius type of relation. Thus, the experimental data shown in Figs. 4.1-4.3 are re-plotted on a semi-log scale to illustrate ln(flux) vs 1/T. This is shown in Figs. 4.4-4.6 for the three salt solutions, respectively.

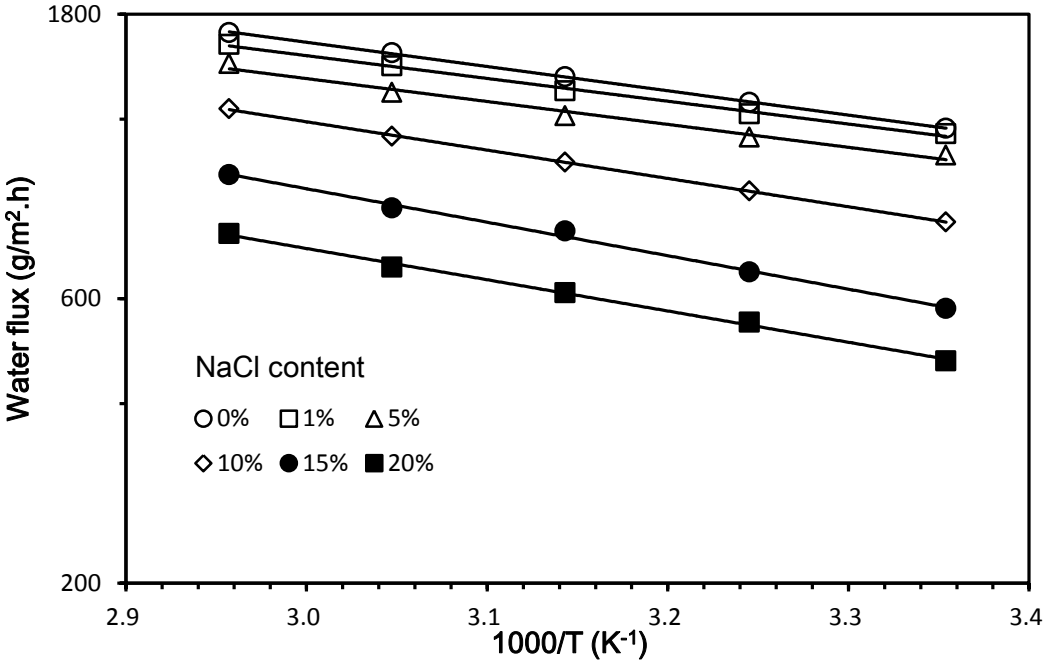

Figure 4.4 Arrhenius plot to show temperature dependence of water flux for pervaporative desalination of water. Salt: NaCl

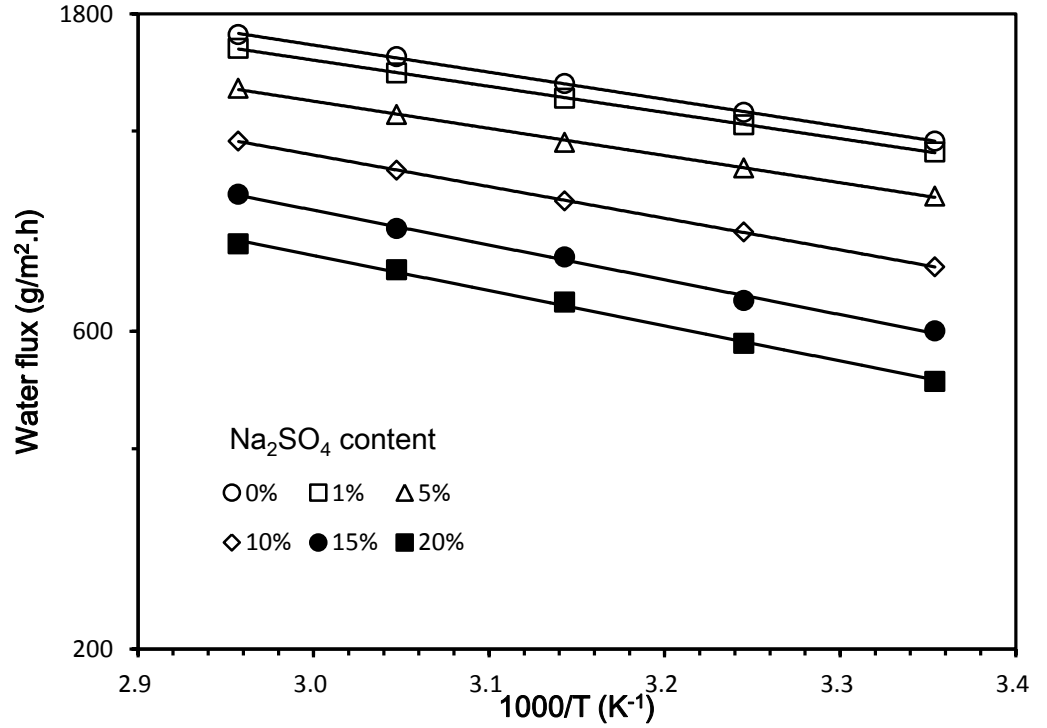

Figure 4.5 Arrhenius plot to show temperature dependence of water flux for pervaporative desalination of water. Salt: Na_2SO_4.

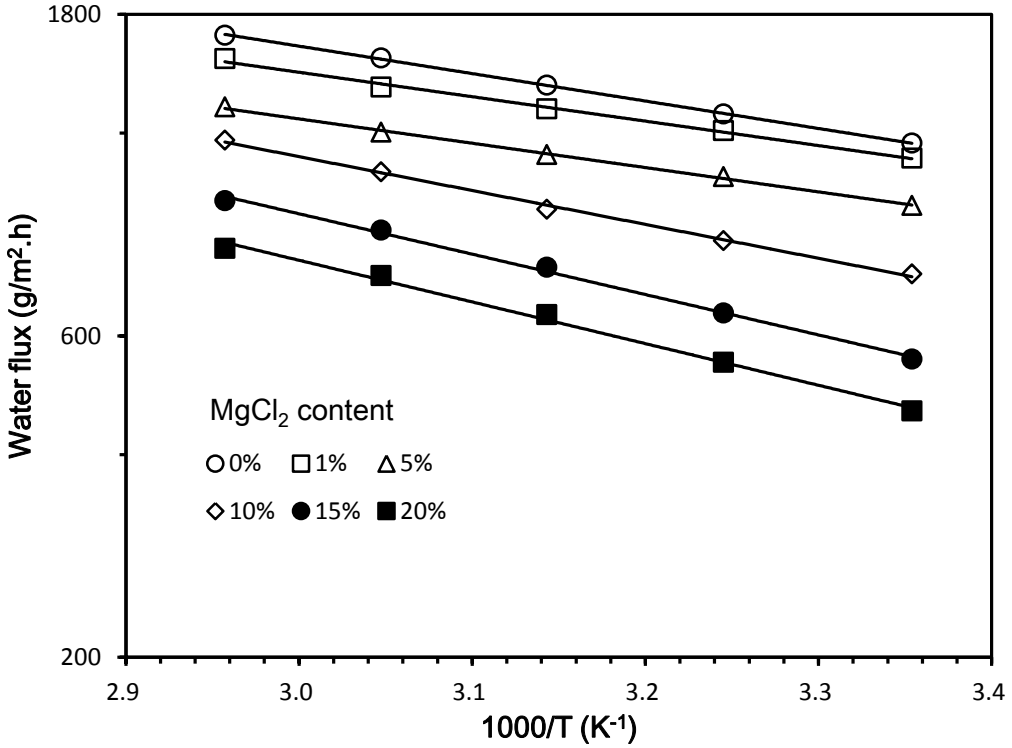

Figure 4.6 Arrhenius plot to show temperature dependence of water flux for pervaporative desalination of water. Salt: $MgCl_2$.

It is shown that there is a linear relationship between the logarithmic water permeation flux and reciprocal temperature. The apparent activation energy, E_J based on temperature dependence of water flux, which represents the overall effects of temperature on mass transfer driving force and membrane permeability, can be calculated from the slope of Arrhenius plot. The activation energy so calculated is shown in Table 4.4.

To separate the effects of temperature on membrane permeability and mass transfer driving force, the permeance of the membrane was evaluated using eq. (2.8). Different from the water flux, the permeance of the membrane to water declined with an increase in the temperature, as shown in Figs. 4.7 to 4.9. As shown in eq. (2.8), the membrane permeance equals to the permeation flux divided by the pressure difference across the membrane (driving force). The

saturated vapor pressure increases with an increase in temperature, which means the driving force increases with temperature. Same trends are also reported elsewhere [Xu et al., 2010]. This indicates that when temperature increases, the increased water flux is due to the increased mass transfer driving force. The decrease in membrane permeance is compensated by the increase in the driving force resulting in a net increase in the water flux. The activation energy of permeation E_P based on membrane permeance which is independent of the effect of temperature on driving force for mass transfer also evaluated from the slopes of the plots in Figs 4.7 to 4.9, and the results are presented in Table 4.5 as well. The heat of vaporization ΔH_V obtained from Aspen plus is also shown in the table. It can be seen that the values of E_J, E_P and ΔH_V, vary with the type of salt, feed salt concentration and temperature. The heat of vaporization (ΔH_V) of water from 25℃ to 65℃ in our study ranges from 42 to 49 (kJ/mol), which is close to the difference between E_J and E_P (i.e., $E_J - E_P$), as suggested by eq. (2.9).

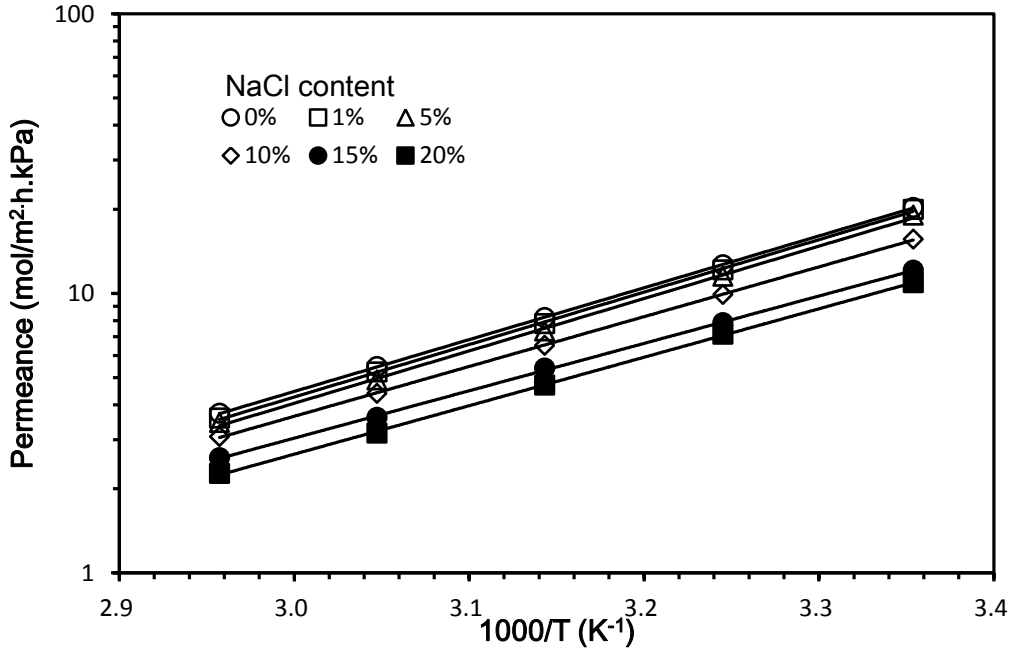

Figure 4.7 Effects of temperature on water permeance in the membrane. Salt in feed, NaCl. Membrane thickness 56µm

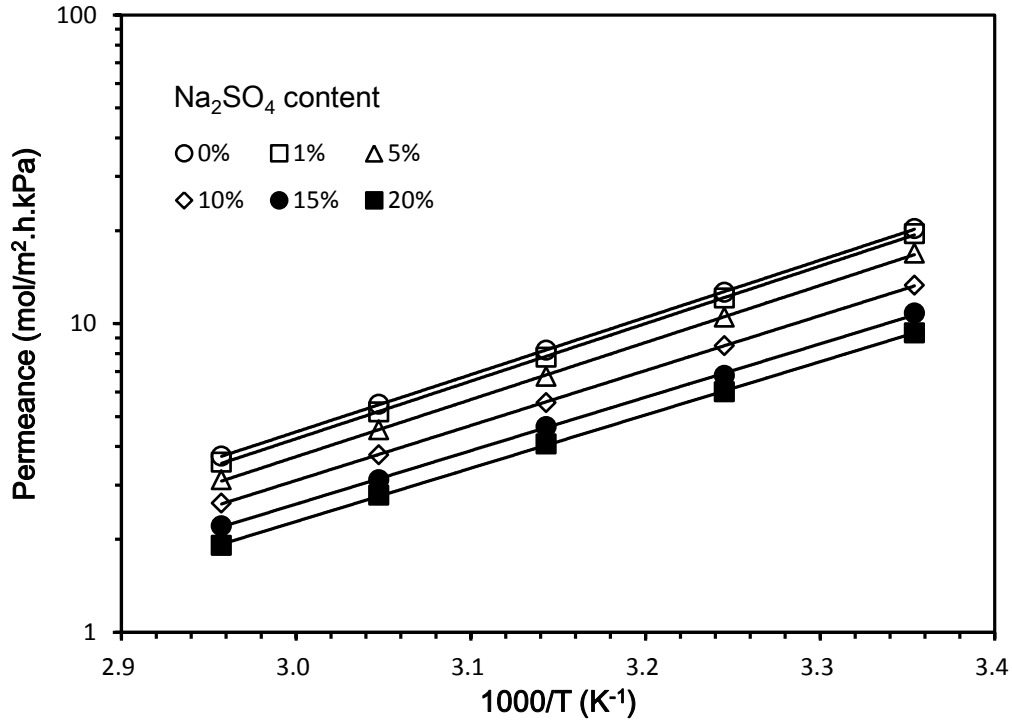

Figure 4.8 Effects of temperature on water permeance in the membrane. Salt in feed, Na2SO4. Membrane thickness 56µm

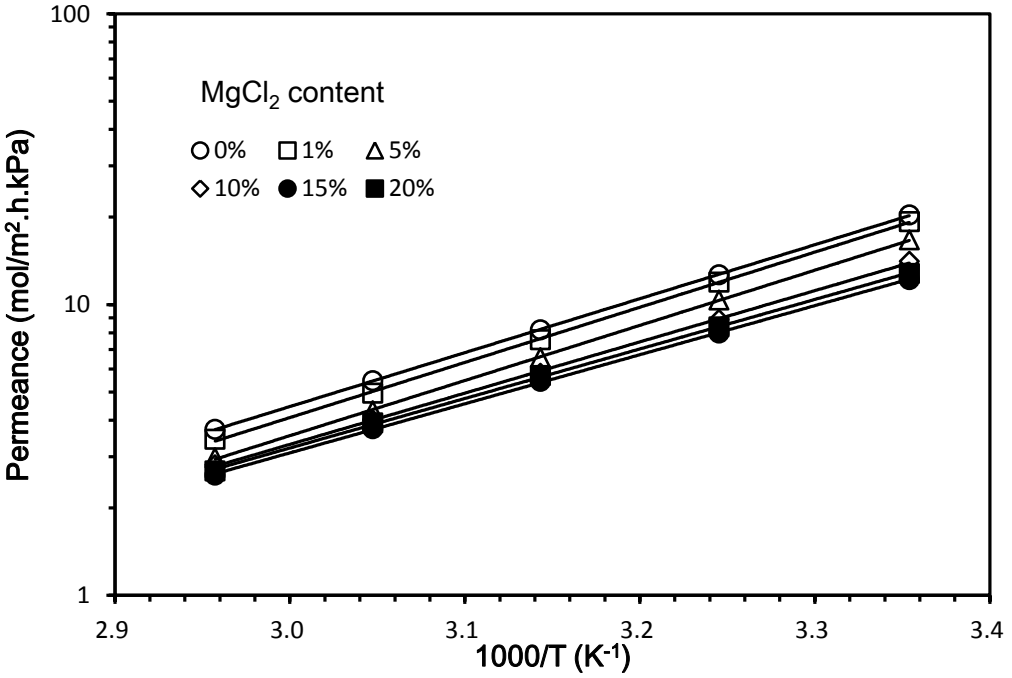

Figure 4.9 Effects of temperature on water permeance in the membrane. Salt in feed, $MgCl_2$.Membrane thickness 56µm

Table 4.5 Activation energies for pure water and different salt solutions with different concentration

	E_J(kJ/mol)	E_P(kJ/mol)	$E_J - E_P$(kJ/mol)	ΔH_V[a] (kJ/mol)
Water	7.80	-35.50	43.30	46.48
NaCl				
1%	7.32	-35.92	43.24	46.34
5%	7.36	-35.87	43.23	45.74
10%	9.10	-34.11	43.21	44.97
15%	10.76	-32.45	43.21	44.15
20%	10.04	-33.19	43.23	43.27
Na_2SO_4				
1%	7.52	-35.72	43.24	46.44
5%	7.82	-35.41	43.23	46.26
10%	9.10	-34.09	43.19	46.05
15%	10.01	-33.15	43.16	44.87
20%	10.12	-33.05	43.17	42.14
$MgCl_2$				
1%	6.94	-36.30	43.24	46.71
5%	6.92	-36.30	43.22	47.67
10%	9.63	-33.72	43.35	47.94
15%	11.47	-32.60	44.07	48.23
20%	11.84	-32.30	44.14	49.53

a: ΔH_V is heat of evaporation of water, which was obtained using Aspen.

4.1.3 Effects of membrane thickness

Eq. (2.1) is valid under the assumption that concentration polarization on the feed side is negligible. Thus, the water flux will be reversely proportional to membrane thickness. To validate this hypothesis, a series of membranes with different thickness (i.e. 39 to 88μm) was used to determine how water flux varies with membrane thickness. The operating temperature was maintained at 25℃, and the results are shown in Figs. 4.10 to 4.12.

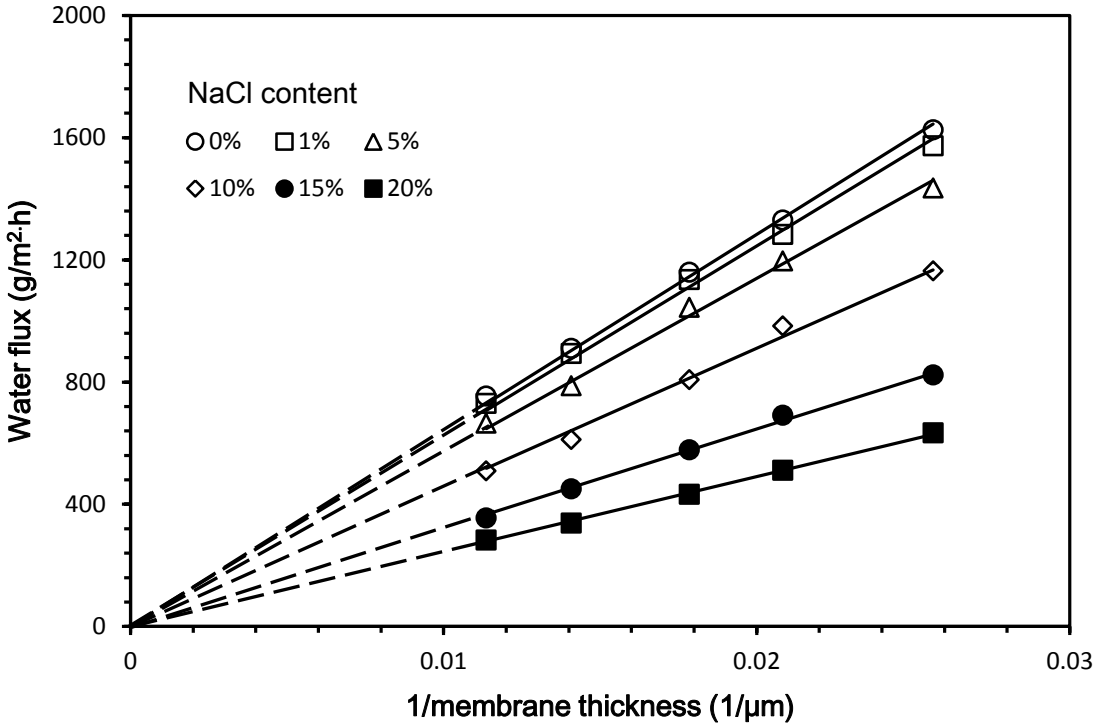

Figure 4.10 Effects of membrane thickness on water flux at different concentrations of NaCl in the feed solution. Temperature, 25℃.

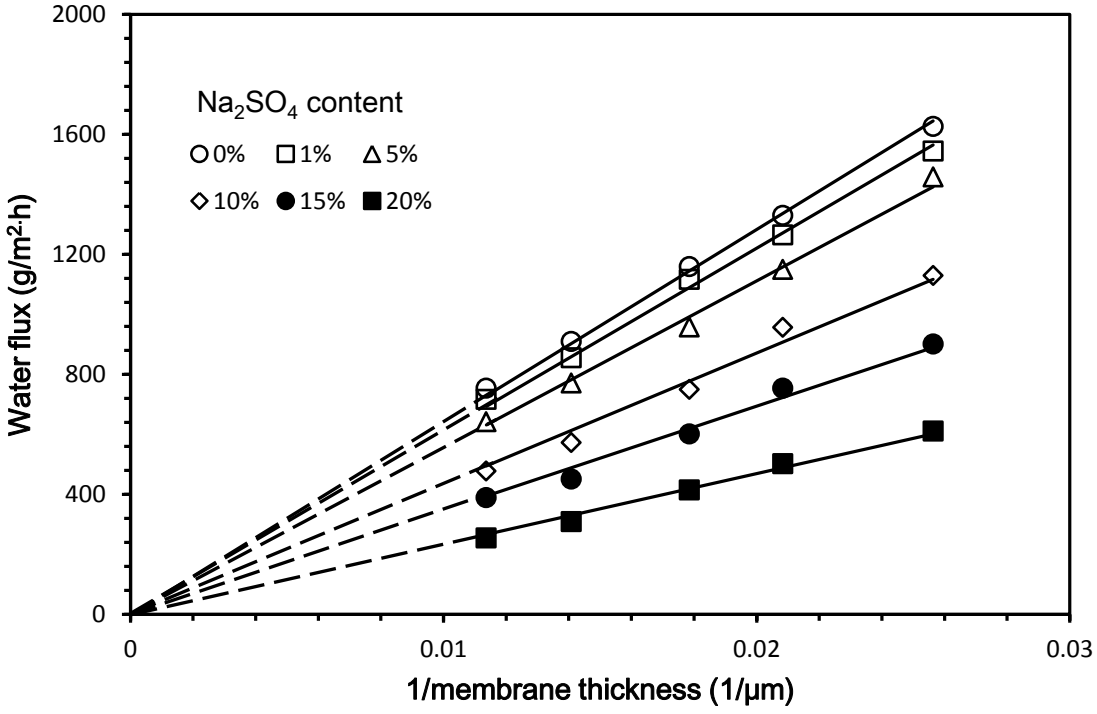

Figure 4.11 Effects of membrane thickness on water flux at different concentrations of Na_2SO_4 in the feed solution. Temperature, 25℃.

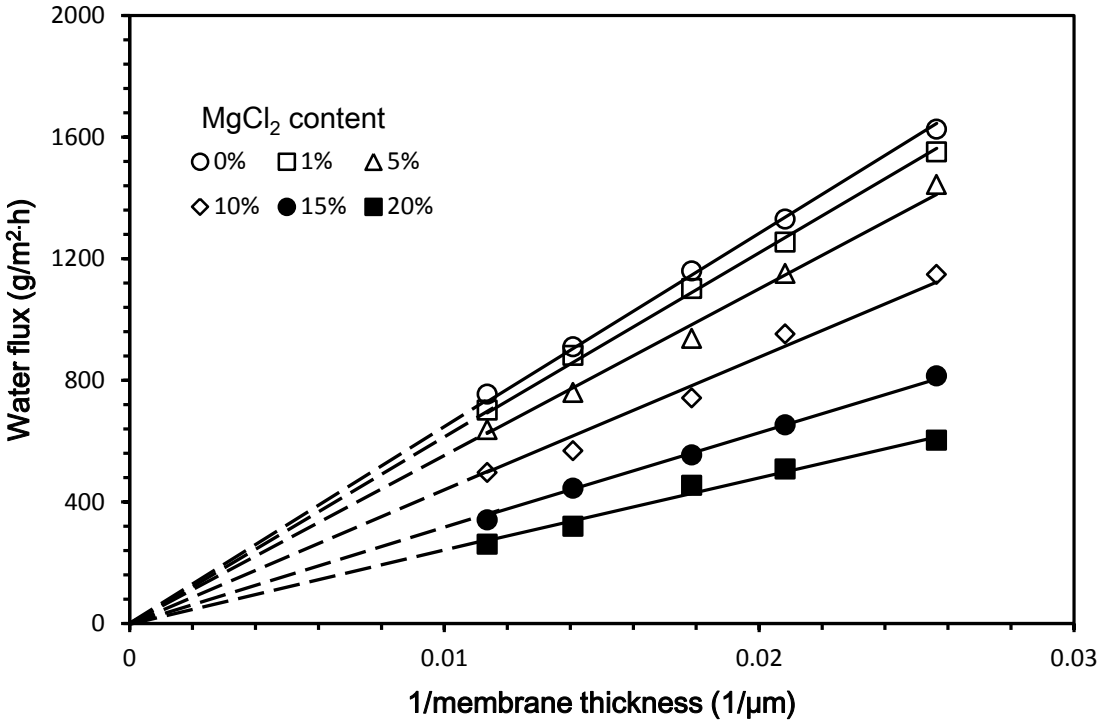

Figure 4.12 Effects of membrane thickness on water flux at different concentrations of $MgCl_2$ in the feed solution. Temperature, 25℃.

As expected, with an increase in membrane thickness from 39 to 88 μm, the pure water flux decreased from 1.62 to 0.79 kg/(m^2.h). It is understandable that the resistance of the membrane to water permeation increased with increasing membrane thickness, resulting in a decrease in water permeation rate.

In addition, there is a linear relationship between the water flux and the reciprocal of membrane thickness for pervaporative desalination of the saline water. The salt rejection remains a high value (>99.9%), and is not affected by the membrane thickness. Based the Fick's law, the diffusivity of a penetrant through a membrane and the permeation flux of this component is related by [Villaluenga et al., 2004]

$$J_i = -D_i \frac{dC_i}{dx} \tag{4.1}$$

where J_i, D_i and C_i are the permeation flux, diffusion coefficient and concentration of

component i, respectively, and x is the diffusion length.

Eq. (4.1) can be integrated as:

$$J_i = D_i \frac{C_{i,f} - C_{i,p}}{l} \quad (4.2)$$

where D_i is the diffusion coefficient of water in the membrane, l is the membrane thickness, $C_{i,f}$ and $C_{i,p}$ are the concentrations of water in the membrane at the feed side and permeate side, respectively. In pervaporatio, the permeate side is at a sufficiently low pressure, and therefore $C_{i,p}$ can be considered to be zero. If the thickness of the membrane does not change during pervaporation process, the diffusion coefficient of water can be expressed as:

$$D_i = \frac{J_i l}{C_{i,f}} \quad (4.3)$$

However, Xie et al., (2011) reported that $C_{i,f}$ to be the concentration of water in the feed solution, which is much more readily available than concentration in the membrane. This is apparently incorrect. The concentration of water in membrane can be determined from water sorption experiments, and this quantity is expected to be related to the water concentration in feed solution via a partition coefficient or solubility coefficient.

The permeability of water P_i in the membrane was calculated from eq. (2.1). At given feed concentration and operating temperature, $\Delta P (= X_i \gamma_i p_i^{sat} - Y_i p^p) \approx X_i \gamma_i p_i^{sat}$ is a constant. Therefore, the permeability of water can be evaluated from the slope of the J vs $1/l$, plot (see Figs 4.10-4.12). The water permeability coefficient so obtained is shown in Fig. 4.13, where the water permeability is expressed in the unit of (mol.m/(m^2.h.kPa)), that is, the quantity of water (in mol) permeated through the membrane per m^2 membrane area per h at 1 kPa transmembrane vapor pressure when the membrane thickness is 1 m.

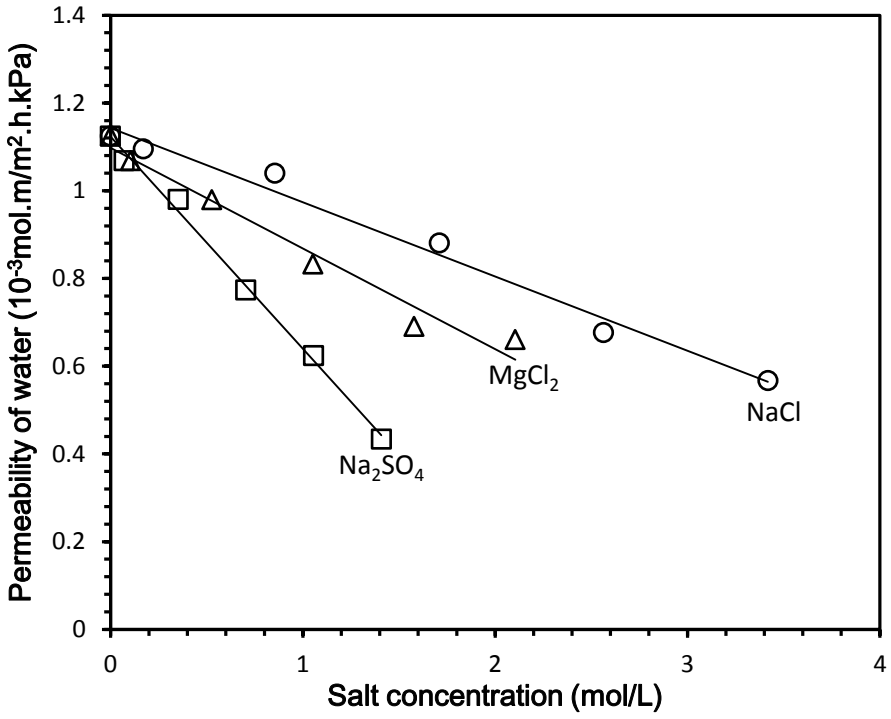

Figure 4.13 Water permeability in the membrane at different feed salt concnetrations. Temperature, 25℃.

As expected, with an increase in salt concentration, the permeability of water in the membrane decreases, and these data match the water permeance in the membrane at 25℃ as determined from pervaporation (Figs 4.7-4.9).

From Fig 4.13, it can be seen that the permeability coefficient of water varies with the salt concentration in water. Based on eq. (2.1), water flux J_w is related to pressure difference $\Delta P = (X_i \gamma_i p_i^{sat} - Y_i p^p)$ could also be drawn. Generally, in pervaporation processes, the permeate pressure can be ignored since it is much lower than the vapor pressure on the feed side. Thus, the water flux J_w is related to $X_i \gamma_i p_i^{sat}$. Fig. 4.14 shows the J_w vs $X_i \gamma_i p_i^{sat}$ at different temperatures. It is not surprising that the plot does not give a linear relationship due to the different water permeability coefficient in the presence of different salts . This again confirmed

that the water permeability coefficient in the membrane is affect by the salts.

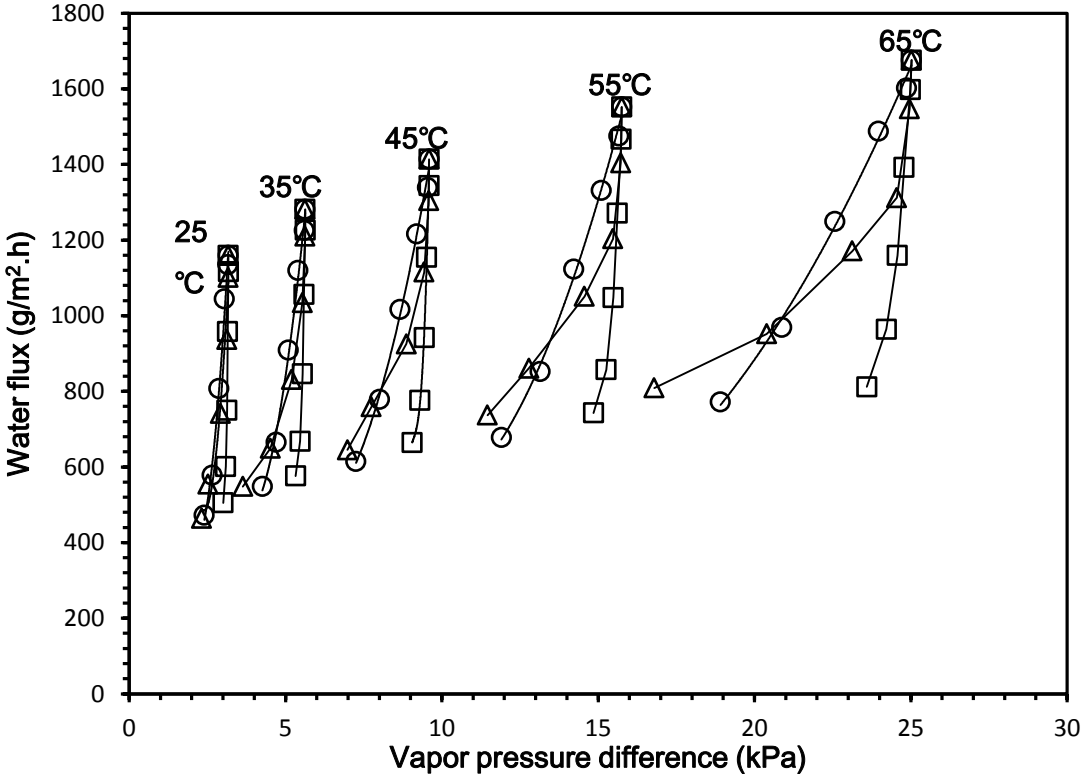

Figure 4.14 Relationship between water flux and vapor pressure of salt solution with different concentrations (0 to 20 wt%) at various temperature (25 to 65 ℃).

4.2 Solubility and permeability of salts in membrane

Because the salts are non-volatile, they were almost fully retained by the membrane in the pervaporation process. However, it does not mean that the membrane is perfectly impermeable to the salts. The solubility and permeability of the salts in the membrane were thus determined experimentally. Solubility is an equilibrium property that represents the ability of the membrane to absorb the permeant. Permeability describes the capability of the membrane to allow certain molecules to pass through by diffusion. Based on the sorption experimental data, the solubilities of water and salt in the membrane were determined. Figs. 4.15 and 4.16 show the salt and water uptakes in the membrane as a function of salt concentration in the liquid solution, respectively.

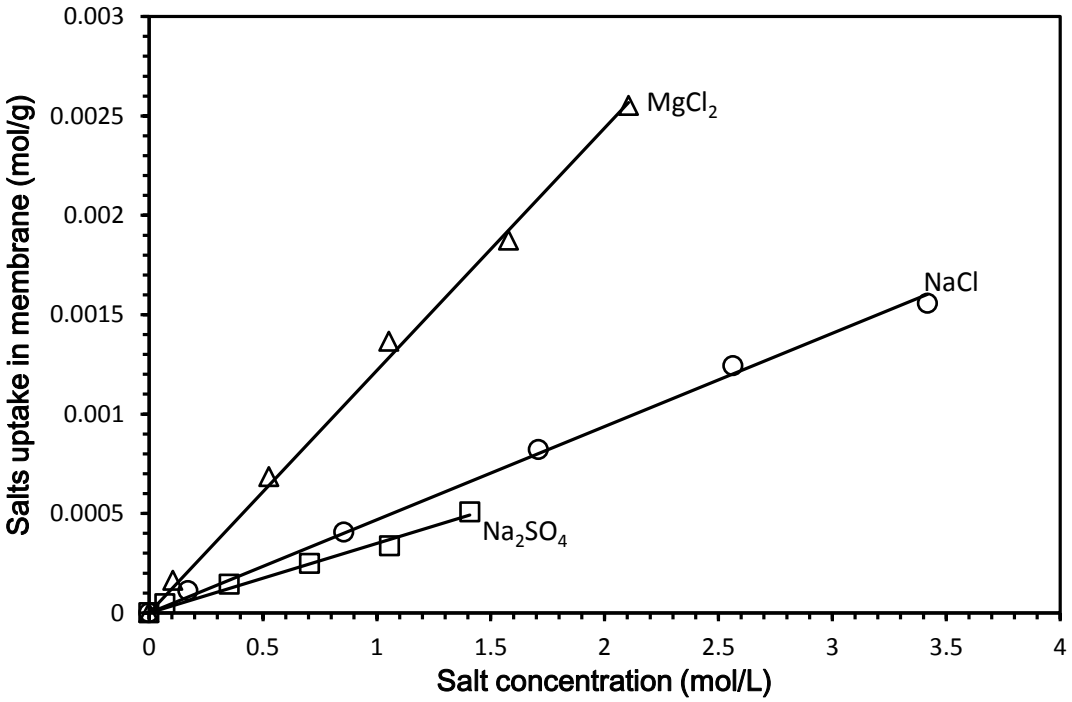

Figure 4.15 Sorption uptake of salts in the membrane at different salt concentrations. Temperature 25℃.

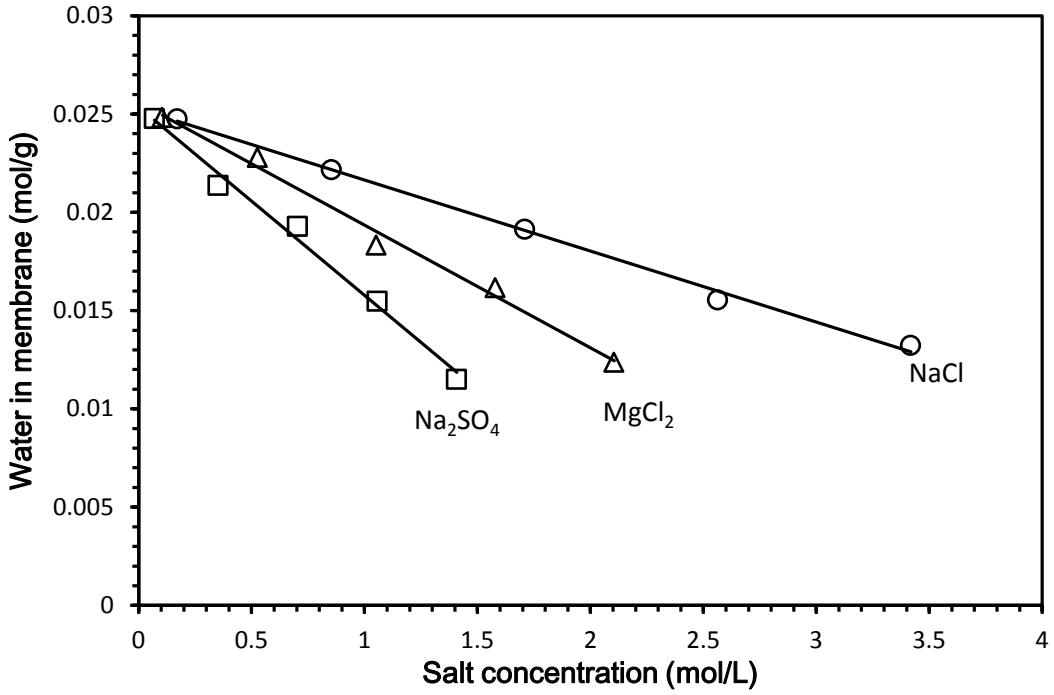

Figure 4.16 Sorption uptake of water in the membrane at different salt concentrations. Temperature 25℃.

To determine the concentration of the species dissolved in the membrane, which will be needed later to estimate diffusivity in the membrane, membrane swelling experiments were also carried out using membrane samples with sizes of 3cm ×3cm. By measuring the thickness, length and width of the membrane, the volume of the membrane can thus be determined. The membrane swelling was expressed as:

$$Swelling = \frac{V_w - V_d}{V_d} \times 100\% \quad (4.5)$$

where V_d and V_w are the volume of membrane before and after the sorption experiment, respectively. Table 4.6 shows the swelling degree of the membrane in different salt solutions at various concentrations at 25℃.

Table 4.6 Swelling degree of the membrane at different salt concentrations. Temperature 25℃.

Compounds	Salt concentration (wt%)	Swelling degree (%)
Water	0	38.24
NaCl solution	1	35.29
	5	29.41
	10	23.53
	15	20.59
	20	17.65
Na_2SO_4 solution	1	33.85
	5	28.18
	10	21.57
	15	20.32
	20	18.71
$MgCl_2$ solution	1	34.31
	5	29.16
	10	23.53
	15	21.14
	20	18.63

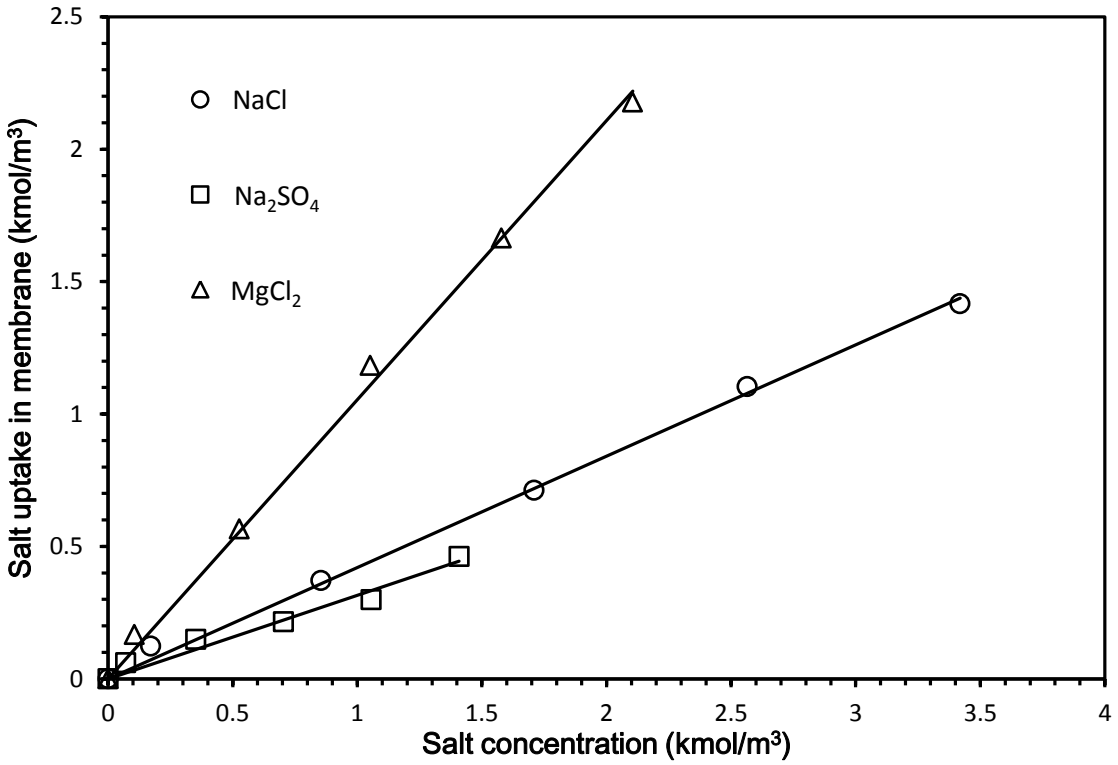

Figure 4.17 Sorption uptake of salts in the membrane at different salt concentrations. Temperature 25℃.

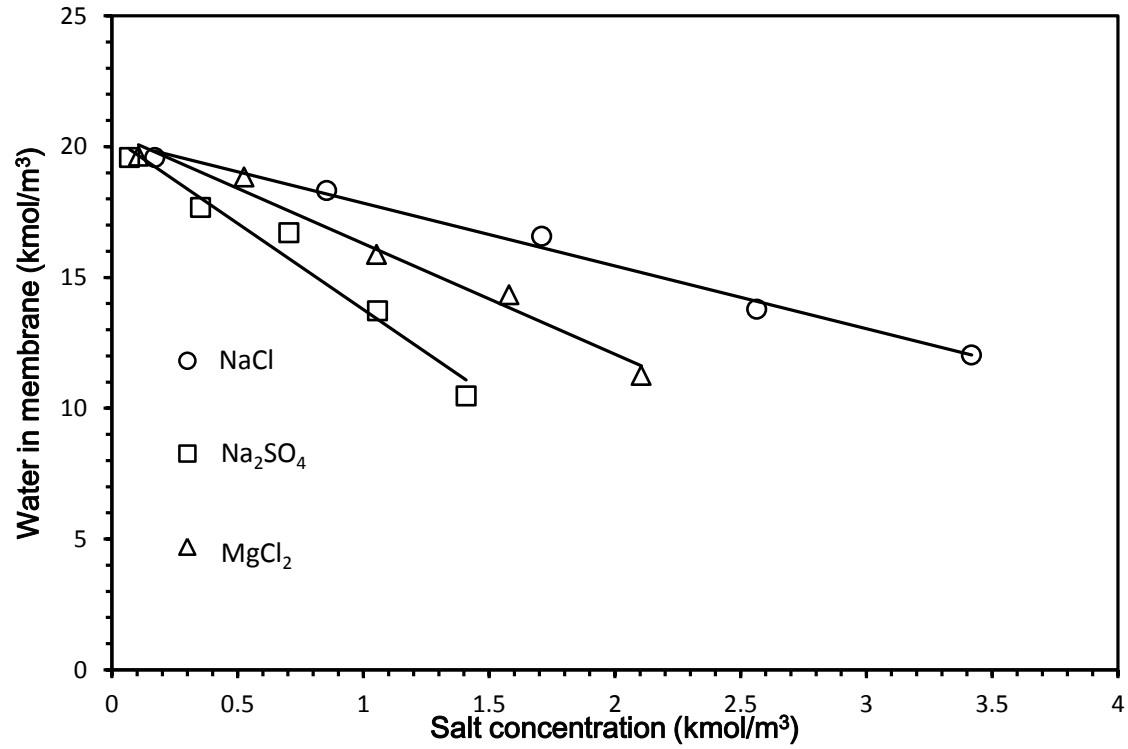

Figure 4.18 Sorption uptake of water in the membrane at different salt concentrations. Temperature 25℃.

Based on the sorption uptake data in Figs 4.15-4.16, the concentrations of salts and water dissolved in the membrane were calculated, and the results are shown in Figs 4.17-4.18. The membrane showed the highest sorption capacity to $MgCl_2$ among the 3 salts studied here. Within the range of feed concentration investigated, the salt sorption is proportional to the salt concentration in feed, a relationship that is similar to the Henry's law, which has been observed for aroma sorption in membranes relevant to aroma enrichment [Mujiburohman, 2008]. Therefore, the solubility coefficients or partition coefficients can be calculated from the slopes of the straight lines, and it was found that the solubility coefficients are 0.421, 0.315, and 1.05 in unit (mol/m^3 membrane)/(mol/m^3 solution), for NaCl, $MgCl_2$ and Na_2SO_4, respectively. Such a unit is sometimes expressed as dimensionless.

An increase in feed concentration led to a decrease in water uptake because the activity of water declined. Interestingly, at a given salt concentration in wt %, the membrane shows a similar water solubility for the different salt solutions.

As mentioned earlier, strictly speaking the approach of Xie et al. (2011) to determine salt diffusivity in the membrane is incorrect. An attempt was thus made to determine the diffusivity and permeability of the salt solutes in the membrane via a series of diffusion experiments. Suppose at time 0 the salt solution was charged to the feed side of the membrane, the quantity of salt in the permeate side will gradually increase with time. Figs 4.19 to 4.21 show the experimental data for the diffusion of different salts through a 56μm thick membrane at various initial salt concentrations.

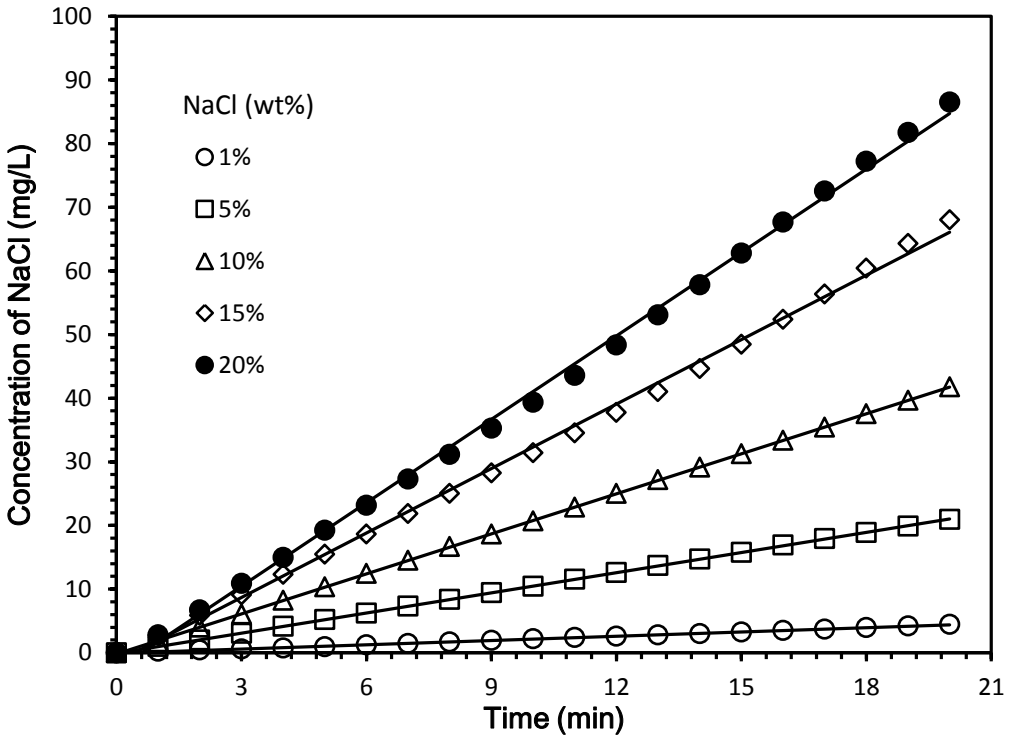

Figure 4.19 Concentration of NaCl in receiving tank as a function of time; membrane thickness 56µm.

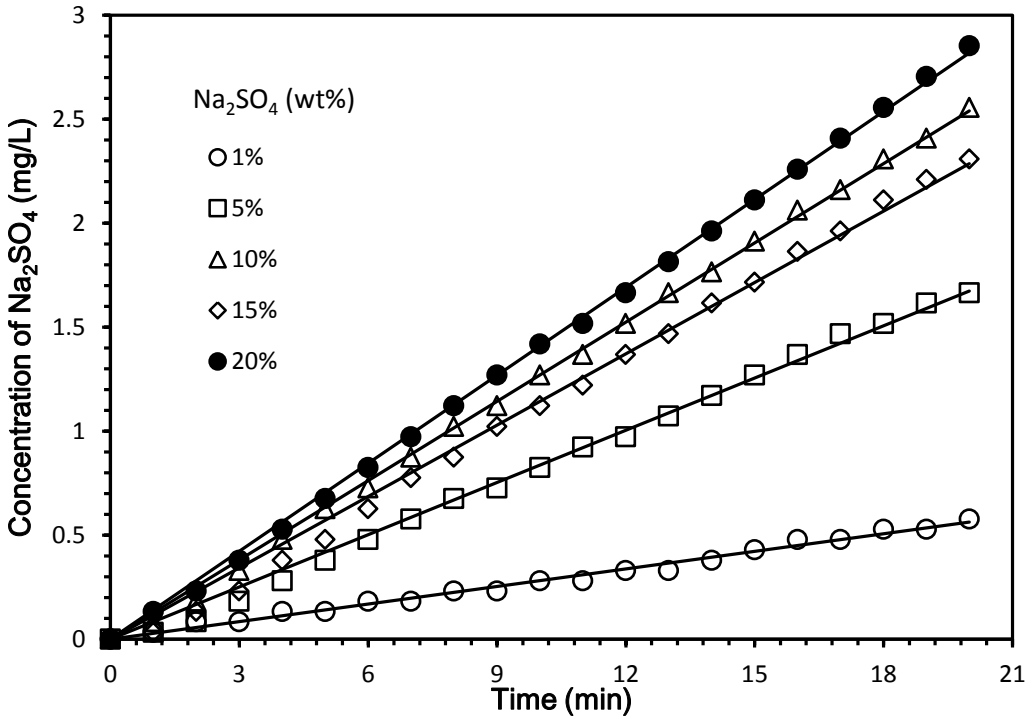

Figure 4.20 Concentration of Na_2SO_4 in receiving tank as a function of time; membrane thickness 56µm.

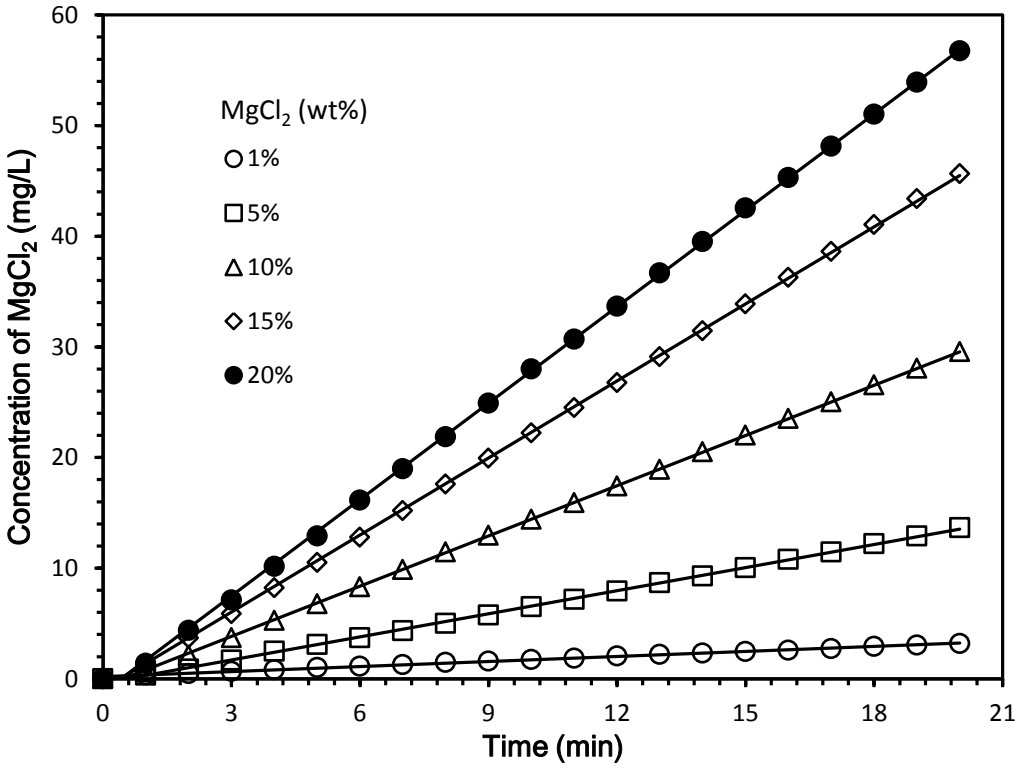

Figure 4.21 Concentration of $MgCl_2$ in receiving tank as a function of time; membrane thickness 56µm.

The time lag in diffusion was unfortunately not determined accurately, and thus salt diffusivity in the membrane could not be evaluated from the time lag. Nonetheless, the permeability coefficients of different salts were evaluated using the quasi steady state permeation using the following equation [Chen et al., 2010]:

$$-\ln\left(\frac{m_0 - V_t C_R}{m_0 - V_t a}\right) = \frac{PA}{l}\left(\frac{1}{V_D} + \frac{1}{V_R}\right)(t - t_0) \qquad (4.4)$$

where m_0 is the total amount of salt in the system, V_D is the volume of donor source, V_R is the volume of the receptor side, $V_t\ (= V_D + V_R)$ is the total volume, a is the salt concentration in the receptor side at time t_0, C_R is the salt concentration in receptor side various with time t, A is the membrane area, l is the membrane thickness. Defining $\mathrm{F(t)} = -\ln[\frac{m_0 - V_t C_R}{m_0 - V_t a}]$, a plot of $\mathrm{F(t)}$ against t will yield a straight line, and the permeability coefficient P of the salt can be

calculated from the slope of the line. Figs 4.22-4.24 show the $F(t) - t$ relationship for NaCl, Na_2SO_4 and $MgCl_2$ diffusion at different initial salt concentrations, respectively.

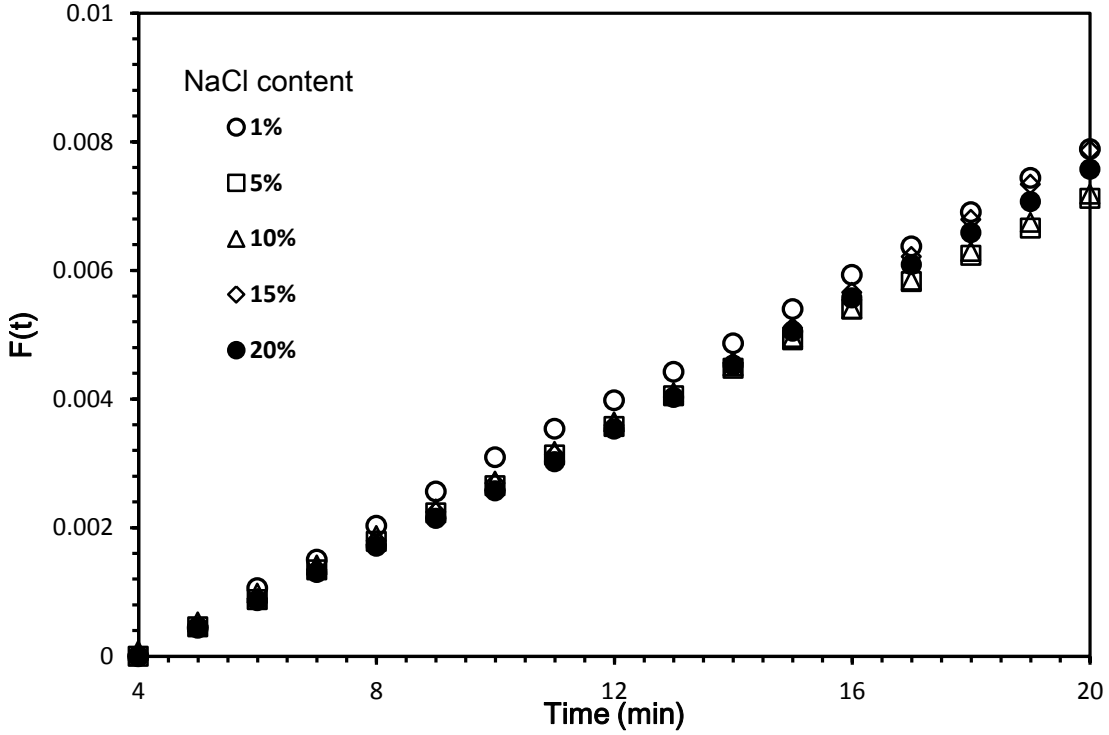

Figure 4.22 The F(t) versus t curves for NaCl diffusion. Membrane thickness 56 µm.

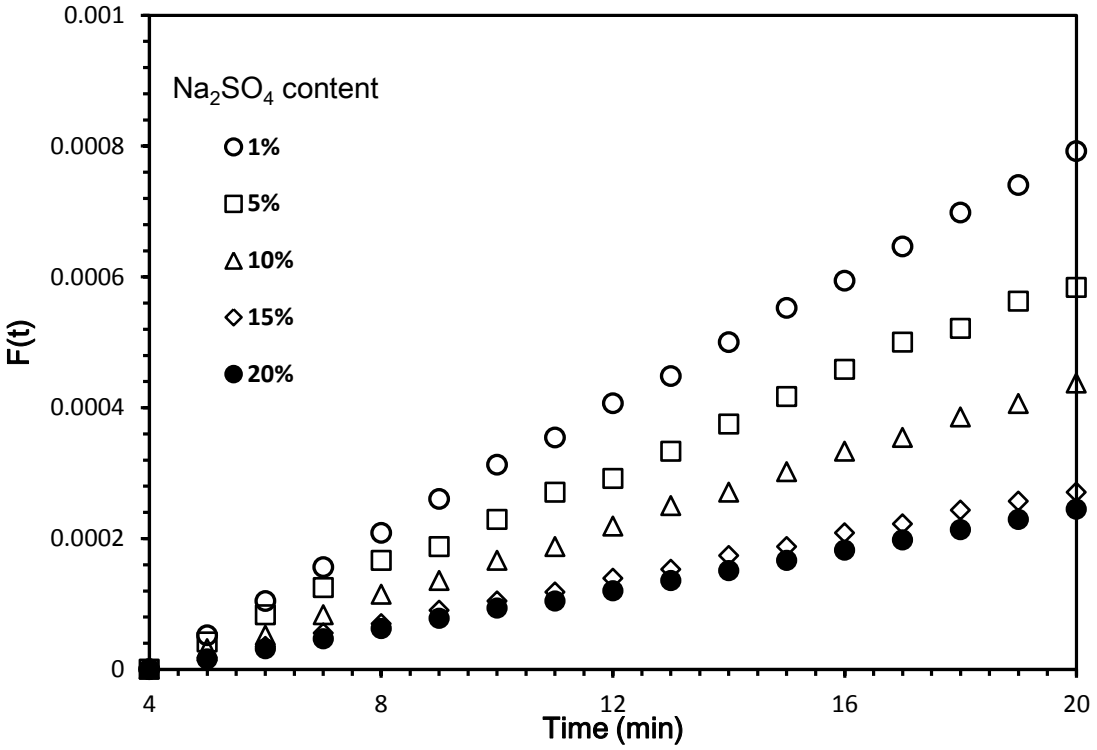

Figure 4.23 The F(t) versus t curves for Na_2SO_4 diffusion. Membrane thickness 56 µm.

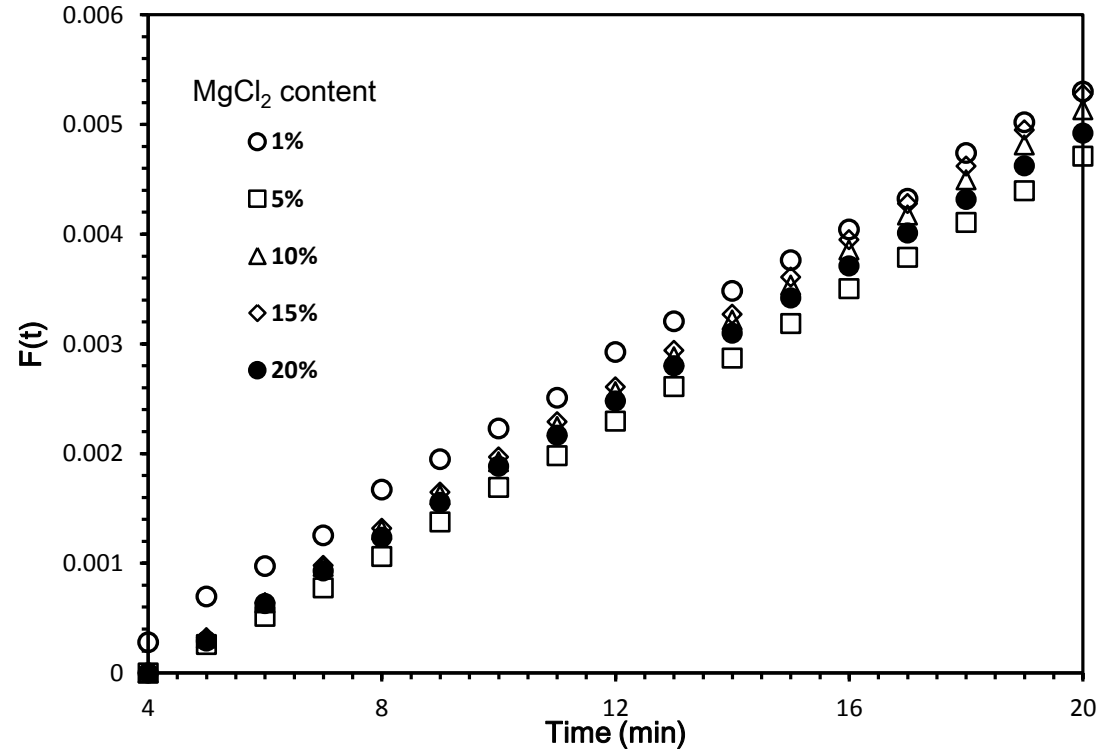

Figure 4.24 The F(t) versus t curves for MgCl2 diffusion. Membrane thickness 56 µm.

In theory, there should be a nonlinear part at the early period on the F(t) vs t cure, due to the impact of transient permeation at the beginning, and this nonlinear part gradually diminishes with an increase in the t_0 selected [Chen et al., 2010]. Choosing a t_0 value of 4 min, the slope of linear part of the $F(t) - t$ plot was used to determine the permeability coefficient of the salt. Fig. 4.25 shows the permeability coefficients of the salts at different salt concentrations. Please note that such permeability coefficients measure the ability of the salt pass through the membrane under a concentration gradient across the membrane. It has a dimension of (mol salt).(m membrane thickness)/[m^2 membrane area.s.(mol salt/m^3 solution)] or [m^2/s], which is commonly used in the literature.

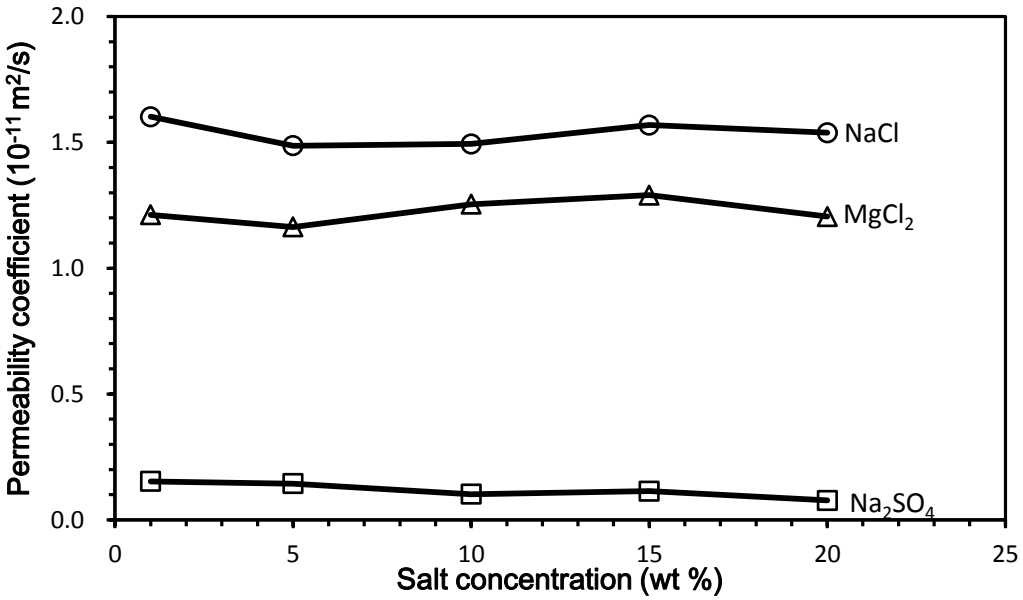

Figure 4.25 Permeability of coefficient of salt in membrane as determined from the diffusion experiments.

As shown in Fig 4.25, NaCl has the highest permeability among the three salts studied, and Na_2SO_4 is the least permeable. In addition, the feed salt concentration has little influence on the permeability of the salts over the salt concentration range investigated here. The salt permeability is related to the ion structure. NaCl, which is the smallest salt, shows the highest permeability coefficient. However, as shown in Fig 4.15, $MgCl_2$ has the highest solubility, and it does not

correspond to a high permeability. This indicates that a high solubility does not mean a high permeability because both solubility and diffusivity are important to the permeability.

When the diffusion coefficient and solubility coefficient are independent of salt concentration, the permeability coefficient P will be equal to the product of diffusion and solubility coefficients, that is, $P = D \cdot S$. Note that solubility coefficient measures how much salt is sorbed in the membrane at a given salt concentration in the solution, and the diffusion coefficient measures how fast the salt diffuses through the membrane under a concentration gradient across the membrane. The diffusivity coefficient can be estimated from $D = P/S$, and the results are shown in Fig 4.26. It can be seen that the diffusivity of the three salts in the membrane follows the order of NaCl >$MgCl_2$ >Na_2SO_4, which is the reverse order of their molecular sizes. Therefore, it may be concluded that the permeability of the salts in the membrane is mainly determined by the diffusion coefficients.

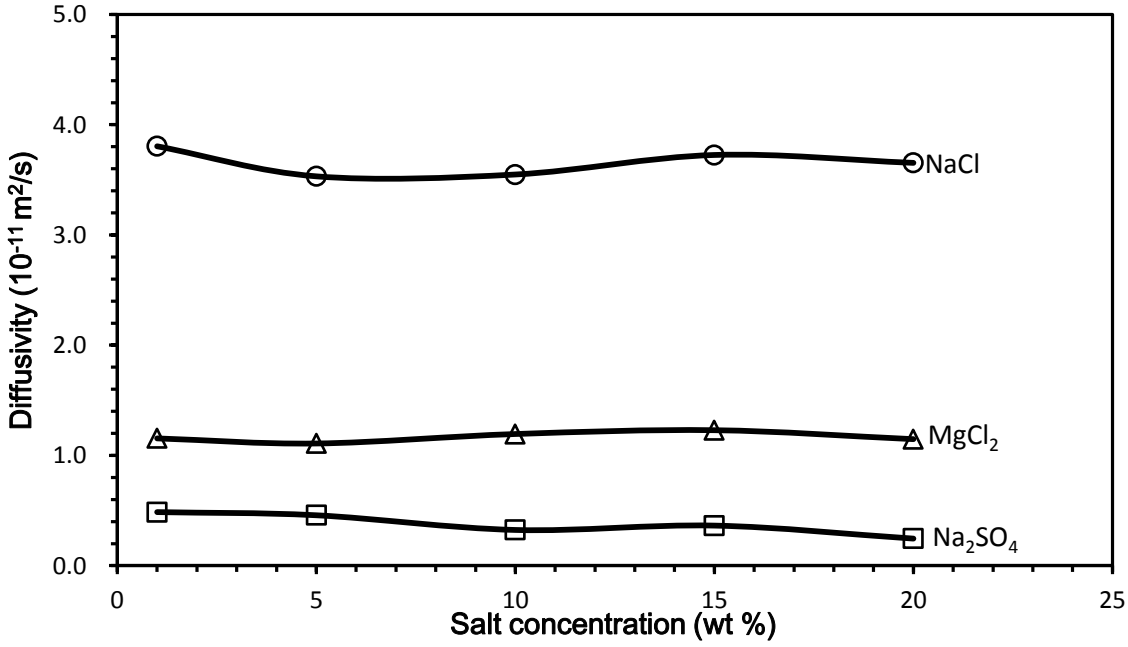

Figure 4.26 Salt diffusivity in the membrane estimated from their solubility and permeability coefficients.

4.3 Concentration profile of salts in membrane during pervaporation

In pervaporative desalination of water, the permeate side is under vacuum. Because the salts are non-volatile, a very high water concentration on the permeate side is achieved. Because of the diffusivity of salts in the membrane, the salt can diffuse in the membrane under a concentration gradient. Thus, it is of interest to investigate the salt concentration profile in the membrane during pervaporation.

Five sheets of membranes with the same thickness of 40μm and area of 22.05 cm^2 were laminated together and then subject to pervaporative desalination of saline water. The pervaporation was continuously conducted for 10 h at room temperature (25℃) with NaCl, $MgCl_2$ and Na_2SO_4 solutions, respectively. Then pervaporation was stopped, and the membrane sheets were quickly delaminated to determine the amounts of salt in each membrane sheet. The salt contents in every membrane sheet and the accumulative sorption amount are shown in Figs 4.27 to 4.29. Here, the number of membrane sheet was counted from the first membrane near the feed side, and the membrane thickness is the total thickness accumulated from the first sheet near the feed side.

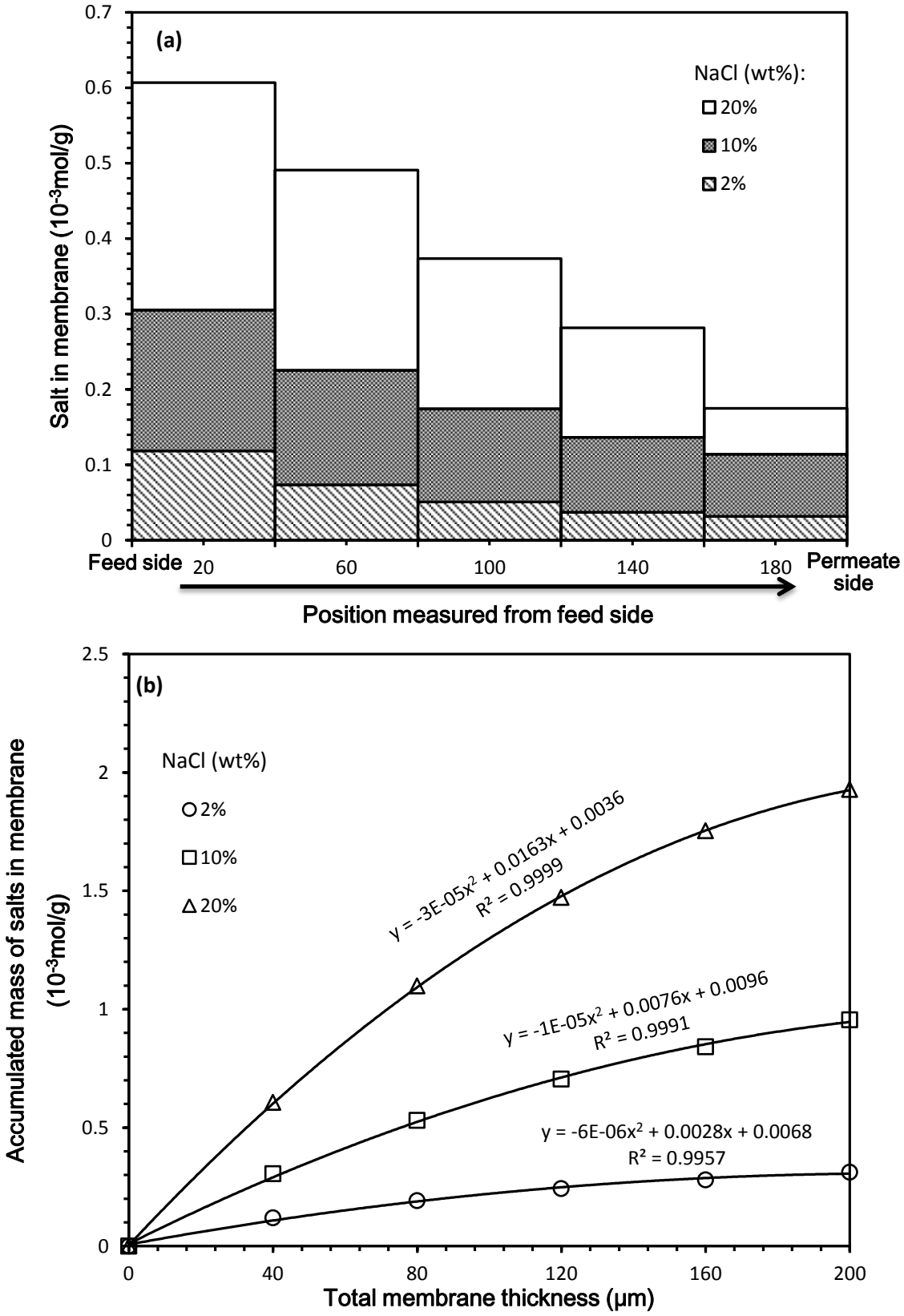

Figure 4.27 Amount of NaCl in each membrane sheet and the accumulated amount of salt in the laminated membranes at different positions.

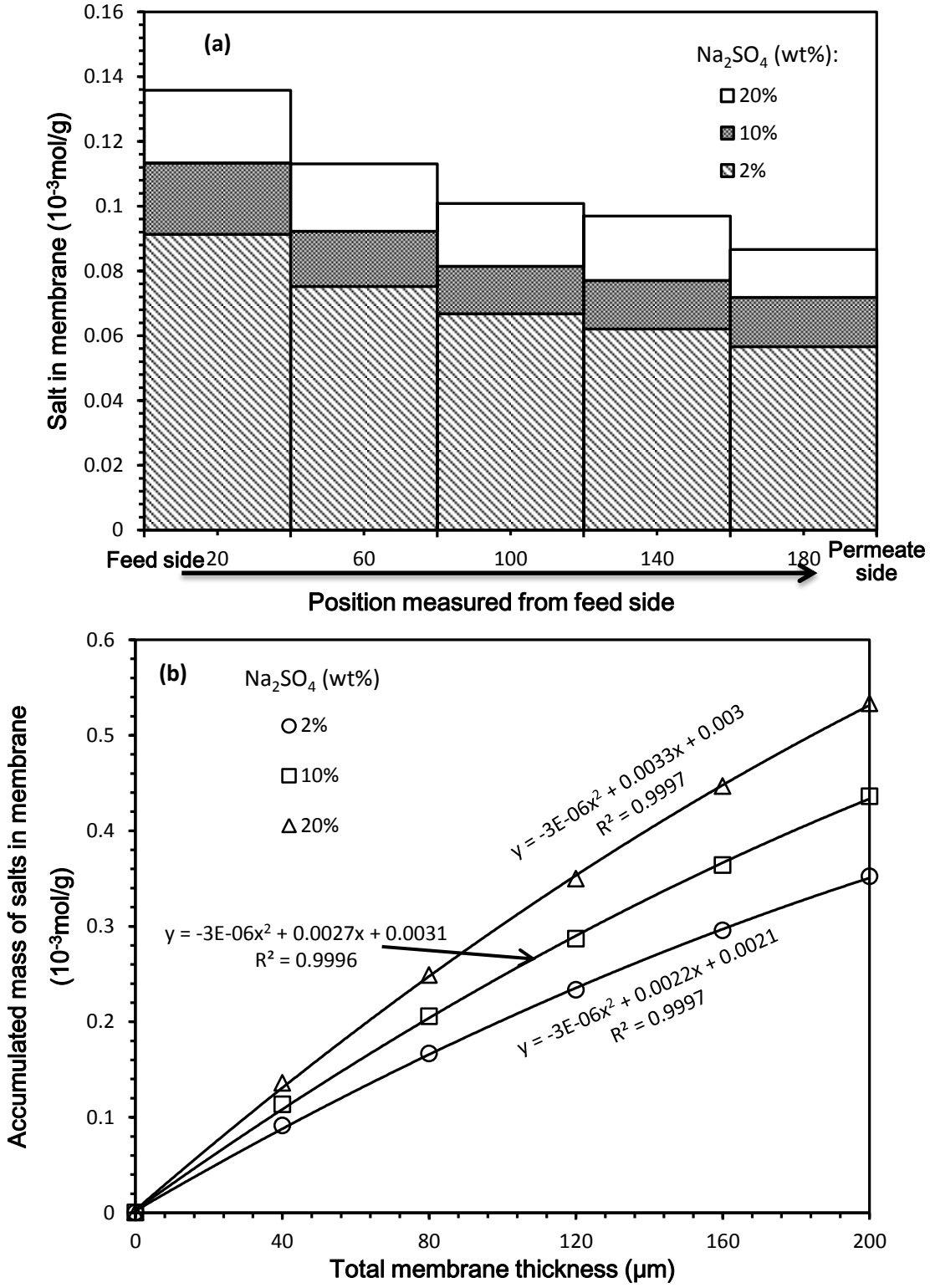

Figure 4.28 Amount of Na_2SO_4 in each membrane sheet and the accumulated amount of salt in the laminated membranes at different positions

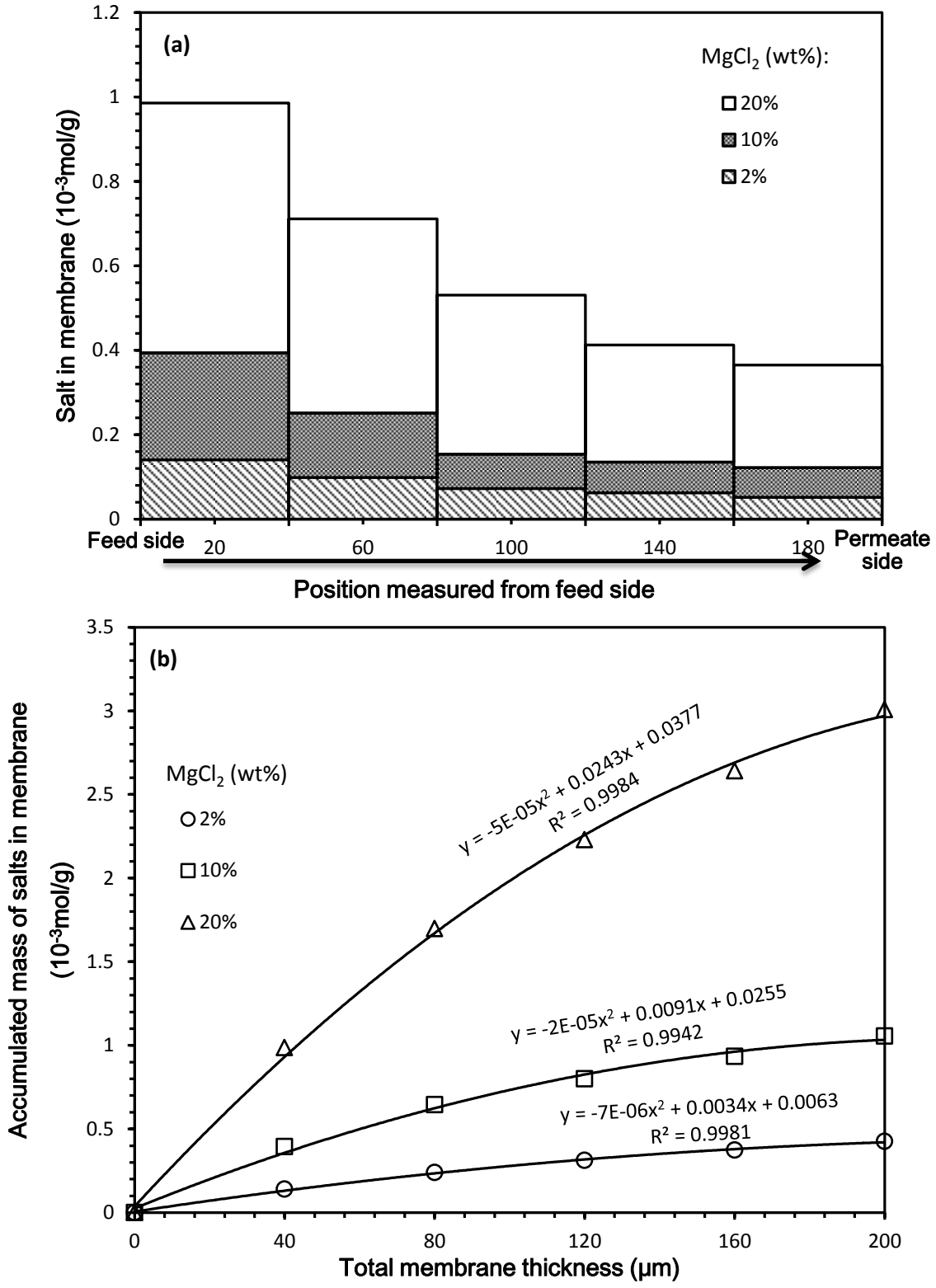

Figure 4.29 Amount of $MgCl_2$ in each membrane sheet and the accumulated amount of salt in the laminated membranes at different positions.

It can be seen from Figs. 4.27 to 4.29 that the salt amount in the membrane decreases from the first layer of the membrane (i.e., the layer which is nearest to the feed side) to the last layer (i.e., the layer which is furthest from the feed side). The accumulative salt in the laminated membrane sheets increases but the increase became less significant along the direction from feed to permeate side. With an increase in the salts concentration, the uptake of salt amount in every single membrane sheet increases, and the accumulative amount of salt uptake in the membrane sheets also increases. It may be hypothesized that the salts are sorbed into the membrane by the following possible mechanisms:

(a) The water molecules permeate through the membrane, the salt ions were dragged into the membrane under the pressure difference applied across the membrane during pervaporation.

(b) Following the solution-diffusion model, both the water and the salt molecules diffuse into the membrane, and water is continuously removed while the salt molecules are left at local positons in the membrane because of their non-volatility.

The accumulated uptake salt in the membrane follows the order of $MgCl_2$ > NaCl> Na_2SO_4, which is in the same order of their solubilities in membrane. It should be noted that the salt solubility, diffusivity and permeability in the membrane discussed earlier are the quantities when the membrane is fully equilibrated with the salt solution. However, in pervaporation where the permeate side is under vacuum, it is expected that the membrane gradually becomes dryer in the direction of pervaporation mass transport. Thus in order to determine the concentration profile of salt in the membrane, the accumulated salt amounts in the membrane as a function of position (Figs. 4.27-4.29) were found to be well represented mathematically by a polynomial function, and a differential was taken with respect to position. The results are shown in Figs. (4.30-4.32),

depicting the concentration profile of the salts in the membrane.

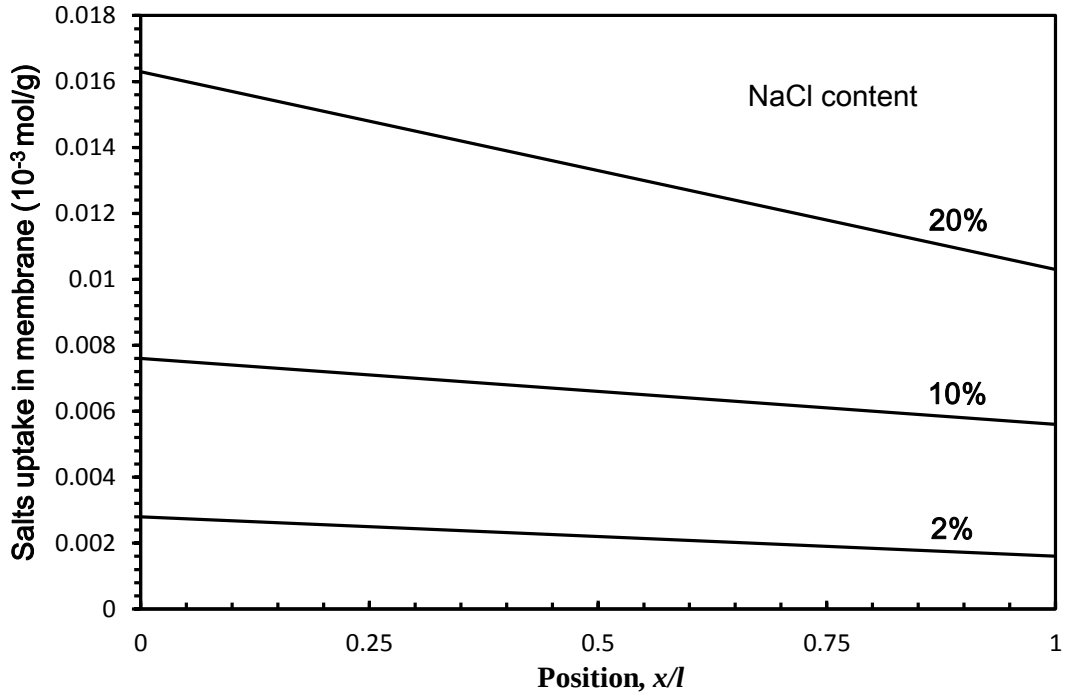

Figure 4.30 Concentration profile of NaCl in the membrane. Temperature 25℃.

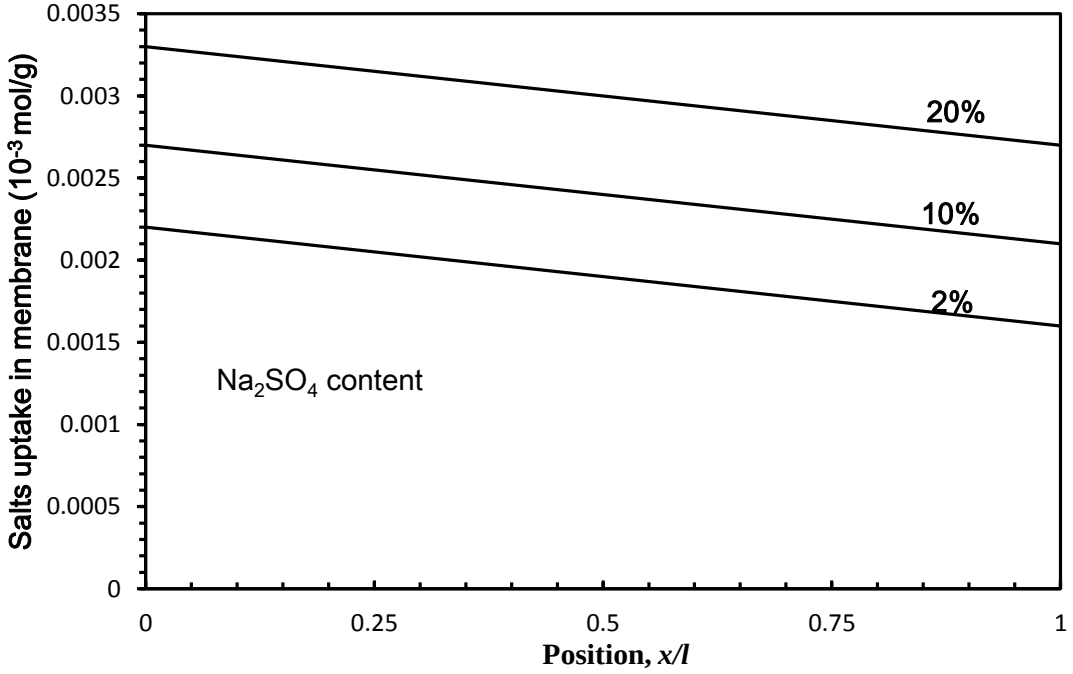

Figure 4.31 Concentration profile of Na_2SO_4 in the membrane. Temperature 25℃.

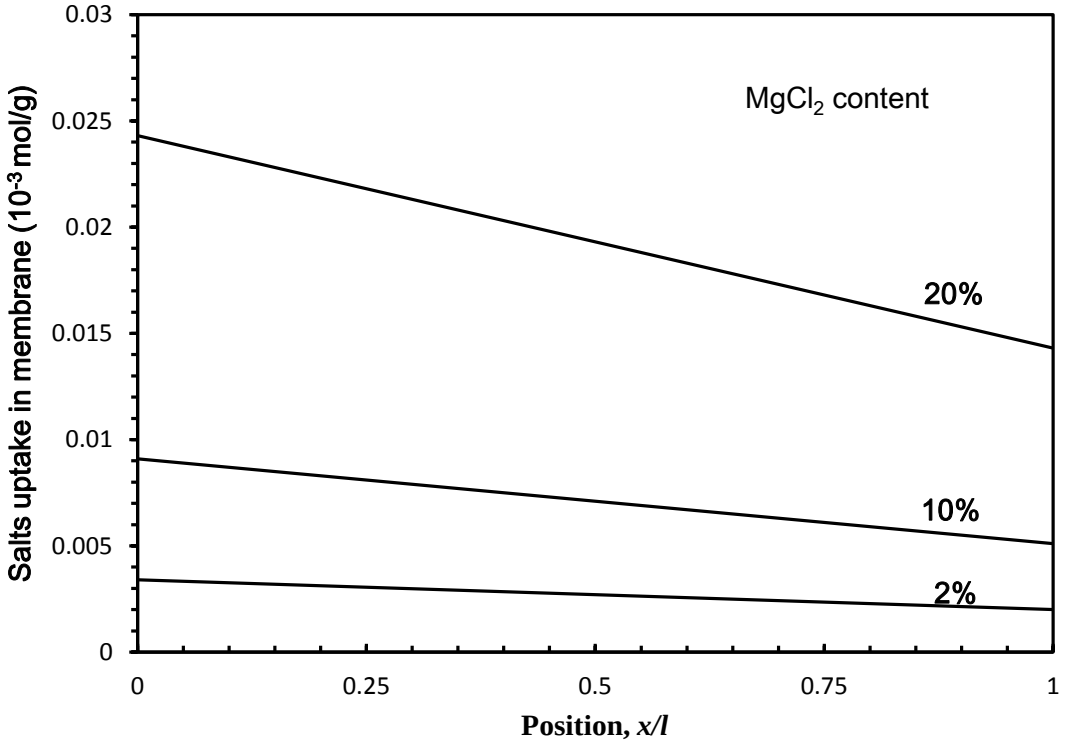

Figure 4.32 Concentration profile of $MgCl_2$ in the membrane. Temperature 25℃.

The linear relationship between the local salt amount and position in the membrane indicates that in spite of gradual change in membrane "wetness" across membrane thickness during the course of pervaporation, the amount of the salt in the membrane varies linearly with the local position. As one may expect, an increase in salt concentration in the feed will result in a higher salt content in the membrane over the entire membrane thickness, as well as a higher salt concentration gradient across the membrane. The high salt concentration gradient across the membrane is unfavorable to the purity of permeate water due to the enhanced driving force for salt transport. On the other hand, the presence of salt in the membrane lowers local concentration of water, which increases the local dryness of the membrane and reduces the membrane permeability to both water and the salt. Caution should be exercised to keep the permeate side under vacuum all the time in order to maintain a high permeate water concentration; the feed

solution should be drained from the membrane unit before vacuum pump is shut down.

4.4 Batch operation tests in pervaporation process

In this part, batch pervaporation experiments were carried out to investigate whether there was any membrane fouling during the course of pervaporation desalination. Three different types of salt solutions (i.e. NaCl, Na_2SO_4 and $MgCl_2$) with different concentrations (1 to 20 wt%) were examined. The operating temperature was maintained as ambient temperature, and the membrane thickness was 39μm. For easy comparison, water normalized flux (J/J_0) was used to represent how water flux changes with time. Here J is the water flux at a given time, and J_0 is the initial water flux at start of experiment. Figs 4.33 shows the water flux measured at different time as pervaporation proceeded batchwise with time.

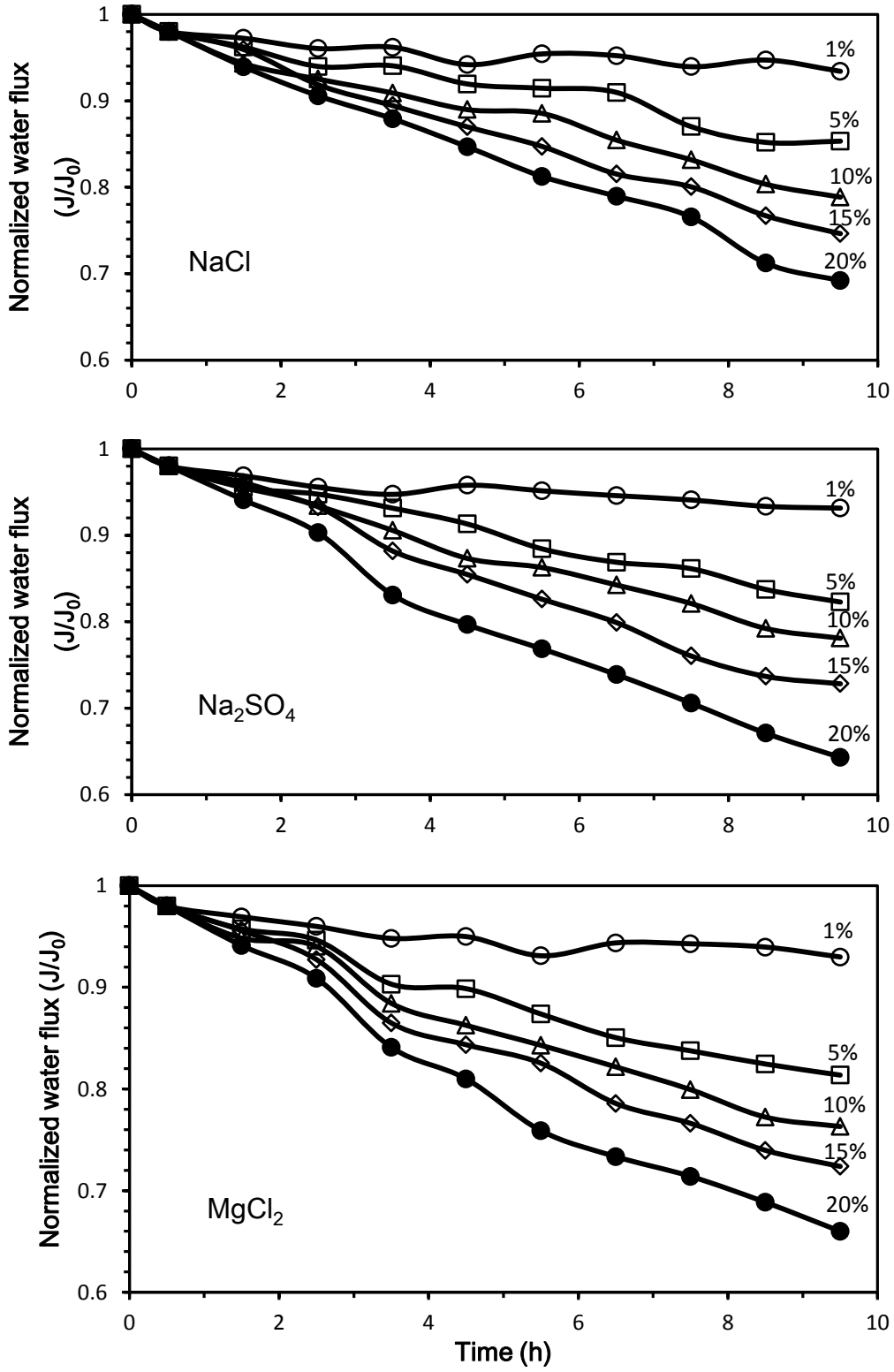

Figure 4.33 Change of water flux with time. Membrane thickness 39μm,temperautre 25℃.

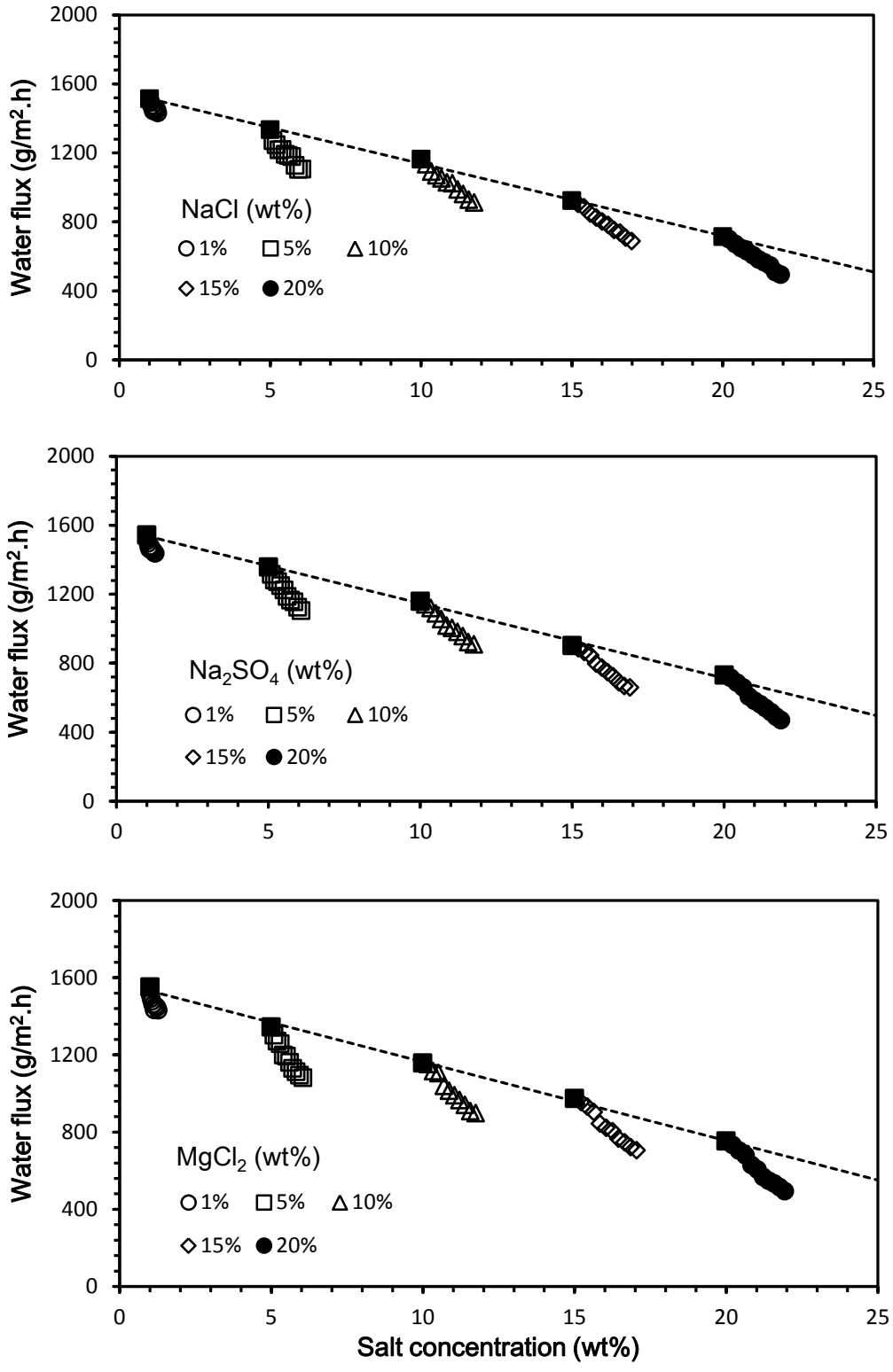

Figure 4.34 The water flux of instantaneous salt concentration in the feed compared with the water flux of batch operation at different feed salt concentrations.

As expected, the water flux declined continuously with the operation time because of increased salt concentration in the feed side, and the flux decline appears to be more severe for the feed solutions with a high salt concentration. For instance, the water flux declined by over 30% at an initial feed salt concentration of 20 wt%, while there was only 5% decrease in water flux when the initial salt concentration in the feed was 1 wt%. When membrane was washed with deionized water after each cycle of 10 hours of operation, both the permeation flux was almost fully recovered to its initial value. Therefore, membrane fouling is shown not to be significant, indicating that at least there was no irreversible fouling. However, if the flux is plotted as function of the instantaneous salt concentration in the feed as shown in Fig 4.34, it does not match well with the experimental data of water flux at different feed salt concentrations obtained previously. A possible reason is that some water vapor in the permeate was lost in the switching of the cold trap under vacuum. A more in-depth study is needed to figure this out. Nonetheless, the batch pervaporation data suggest that the membrane is stable over a pro-longed period of operation, which is of significant interest from an application point of view.

Chapter 5

Conclusions and Recommendations

5.1 Conclusions

This work dealt with pervaporative desalination of high salinity water. The water permeability in the membrane was investigated. The solubility, diffusivity and permeability of the salts in the membrane was also studied. It was shown that the pervaporative desalination was effective, and a high purity water (>99.9%) was produced as permeate. The following conclusions can be drawn from the study:

(1) The membrane exhibited an outstanding performance for desalination of high-salinity water. The pure water flux reached 1676 g/(m^2.h) and the salt rejection achieved >99.9% at 65℃. The water flux increased from 1160 g/(m^2.h) to 1680 g/(m^2.h) with an increase in temperature from 25℃ to 65℃,and the temperature dependence of water flux obeyed an Arrhenius type of relationship.

(2) The water flux decreased with an increase in the salinity of the feed water. Increasing the feed salt concentration from 1 to 20 wt% resulted in a ~50% reduction in water flux, whereas the salt rejection was not influenced. The salt type (i.e., NaCl, Na_2SO_4 and $MgCl_2$) was found to have little effect on the water flux at given salinity of the feed water.

(3) The water flux decreased with an increase in the membrane thickness, whereas the salt rejection was not influenced. It has experimentally confirmed that water flux was inversely proportional to membrane thickness, indicating concentration polarization during the pervaporative desalination was insignificant. In addition, the water permeability coefficient

decreased with an increase in the salt concentration in the feed solution.

(4) The solubility of the salts in the membrane followed the order of $MgCl_2$>NaCl>Na_2SO_4. On the other hand, the permeability of the salts in the membrane was not influenced by the feed salt concentration, and the salt permeability followed the order of NaCl>$MgCl_2$>Na_2SO_4.

(5) The salts would penetrate into the membrane during the pervaporation process, and the salt concentration in the membrane varied linearly with position. To our knowledge, this is the first time the salt concentration profile in the membrane was determined experimentally. A high purity water was obtained as permeate as long as the permeat side was kept dry under vacuum so that the salt in the membrane would not be removed to the permeate during pervaporation.

(6) Batch operation of pervaporative desalination was tested, and flux decline over time was due to increased salt concentration on the feed side. Neither membrane fouling nor concentration polarization was significant.

5.2 Recommendations

Based on this research, the following recommendations can be for further studies to look into the desalination by pervaporation using the Pebax membrane:

(1) In industrial wastewater treatment, pH value is an important factor that may affect the membrane performance. Therefore, the effects of pH value of feed water on the desalination performance of the membrane should be investigated.

(2) As water flux increases when membrane thickness is reduced, it is desirable to develop composite membranes with much thinner membrane effective layer thickness in order to further increase the water flux but maintain the high salt rejection.

(3) The Peabx polymer has crystalline PA phase which provides mechanical stability to the membrane, and a more permeable amorphous PE phase. Tailoring the PA and PE segments in the membrane to maximize the permeability while retaining sufficient strength of the membrane would be meaningful.

(4) In practical applications, there are very often more than salts present in the saline water, a study of pervaporative desalination of saline water with multiple salts is needed to understand how the interactions between the salts would affect the overall desalination performance of the membrane.

References

An, W., X. Zhou, X. Liu, P.W. Chai, T. Kuznicki, S.M. Kuznicki, "Natural zeolite clinoptilolite-phosphate composite membranes for water desalination by pervaporation" , *J. Membr. Sci*., 470 (2014) 431-438.

Alkhudhiri, A., N. Darwish, N. Hilal, "Membrane distillation: A comprehensive review", *Desalination*, 287 (2012) 2-18.

Al-Rawajfeh, A.E., "Nanofiltration pretreatment as CO_2 deaerator of desalination feed: CO_2 release reduction in MSF distillers", *Desalination*, 380 (2016) 12-17

Avlonitis, S.A., K. Kouroumbas, N. Vlachakis, "Energy consumption and membrane replacement cost for seawater RO desalination plants", *Desalination*, 157 (2003) 151-158.

Bondar, V.I., B.D. Freeman, I. Pinnau, "Gas sorption and characterization of poly (ether-b-amide) segmented block copolymers", *J. Polym. Sci.: Polym. Phy*., 37 (1999) 2463-2475.

Catarino, M., A. Ferreira, A. Mendes, "Study and optimization of aroma recovery from beer by pervaporation", *J. Membr. Sci*., 341 (2009) 51-59.

Chai, L., H. Li, X. Zheng, J. Wang, J. Yang, J. Lu, D. Yin, Y. Zhang, "Pervaporation separation of ethanol-water mixtures through B-ZSM-11 zeolite membranes on macroporous supports", *J. Membr. Sci*., 491 (2015) 168-175.

Chaudhri, S.G., B.H. Rajai, P.S. Singh, "Preparation of ultra-thin poly(vinyl alcohol) membranes supported on polysulfone hollow fiber and their application for production of pure water from seawater", *Desalination*, 367 (2015) 272–284.

Chen, Y., Y. Zhang, X. Feng, "An improved approach for determining permeability and diffusivity relevant to controlled release", *Chem. Eng. Sci*., 65 (2010) 5921-5928.

Choudhury, J.P., P. Ghosh, B.K. Guha, "Separation of ethanol from ethanol—water mixture by reverse osmosis", *Biotechnol. Bioeng*., 27 (1985) 1081-1084.

Cho, C.H., K.Y. Oh, S.K. Kim, J.G. Yeo, P. Sharma, "Pervaporative seawater desalination using NaA zeolite membrane: mechanisms of high water flux and high salt rejection", *J. Membr. Sci*., 371 (2011) 226-238.

Chong, T.H., S.L. Loo, W.B. Krantz, "Energy-efficient reverse osmosis desalination process", *J. Membr. Sci*., 473 (2015) 177-188.

Choudhari, S.K., F. Cerrone, T. Woods, K. Joyce, V. O'Flaherty, K. O'Connor, R. Babu, "Pervaporation separation of butyric acid from aqueous and anaerobic digestion (AD)

solutions using PEBA based composite membranes", *J. Ind. Eng. Chem*., 23 (2015) 163-170.

Drobek, M., C. Yacou, J. Motuzas, A. Julbe, L. Ding, J.C.D. da Costa, "Long term pervaporation desalination of tubular MFI zeolite membranes", *J. Membr. Sci*., 415-416 (2012) 816-823.

Duke, M.C., J. O'Brien-Abraham, N. Milne, B. Zhu, J.Y.S. Lin, J.C.D. da Costa, J "Seawater desalination performance of MFI type membranes made by secondary growth", *Sep. Purif. Technol*., 68 (2009) 343-350.

Elimelech, M. and W.A. Phillip, "The future of seawater desalination: energy, technology, and the environment", *Science*, 333 (2011) 712-717.

Feng, X. and R.Y.M. Huang, "Estimation of activation energy for permeation in pervaporation precesses", *J. Membr. Sci*., 118 (1996a) 127-131.

Feng, X. and R.Y.M. Huang, "Pervaporation with chitosan membranes. I. Separation of water from ethylene glycol by a chitosan/polysulfone composite membrane", *J. Membr. Sci*., 116 (1996b) 67-76.

Feng, X. and R.Y.M. Huang, "Liquid separation by membrane pervaporation: a review", *Ind. Eng. Chem. Res.* 36 (1997) 1048-1066.

Fouad, E.A. and X. Feng, "Pervaporative separation of n-butanol from dilute aqueous solutions using silicalite-filled poly (dimethyl siloxane) membranes", *J. Membr. Sci*., 339 (2009) 120-125.

Fritzmann, C., J. Lowenberg, T. Wintgens, T. Melin, "State-of-the-art of reverse osmosis desalination", *Desalination*, 216 (2007) 1-76.

Global Water Intelligence, "Desalination industry enjoys growth spurt as scarcity starts to bite" www.globalwaterintel.com , retrieved Jan 2016.

Han, Y., K. Wang, J. Lai, Y. Liu, " Hydrophilic chitosan-modified polybenzoimidazole membranes for pervaporation dehydration of isopropanol aqueous solutions", *J. Membr. Sci*., 463 (2014) 17-23.

Huang, R.Y.M., (Ed), "Pervaporation membrane separation processes", Elsevier, Amsterdam, 1991.

Huang, R.Y.M. and X. Feng, "Pervaporation of water/ethanol mixtures by an aromatic polyetherimide membrane", *Sep. Sci. Technol*., 27 (1992) 1583-1597.

Henthorne, L. and J. Wodehouse, "The science of membrane technology to further enhance oil recovery", *SPE Improved Oil Recovery Symposium*, Society of Petroleum Engineers, 2012.

Huth, E., S. Muthu, L. Ruff, J.A. Brant, "Feasibility assessment of pervaporation for desalinating high-salinity brines", *J. Water Reuse Desal*., 4 (2014) 109-124.

Jonquières, A., Clément, R., Lochon, P., "Permeability of block copolymers to vapors and liquid", *Prog. Polym. Sci*., 27 (2002) 1803-1877.

Jullok, N., R.V. Hooghten, P. Luis, A. Volodin, C.V. Haesendonck, J. Vermant, B.V. Bruggen, "Effect of silica nanoparticles in mixed matrix membranes for pervaporation dehydration of acetic acid aqueous solution: plant-inspired dewatering systems", *J. Clean. Prod*., 112 (2016) 4879-4889.

Kawedia, J.D., V.G. Pangarkar, K. Niranjan, "Pervaporative stripping of acetone, butanol and ethanol to improve ABE fermentation", *Bioseparation*, 9 (2000) 145-154.

Kedem, O., "The role of coupling in pervaporation", *J. Membr. Sci*., 47 (1989) 277-284.

Khajavi, S., J.C. Jansen, F. Kapteijn, "Production of ultra pure water by desalination of seawater using a hydroxy sodalite membrane", *J. Membr. Sci*., 356 (2010) 52-57.

Kujawskia, W., S. Krajewska, M. Kujawski, "Pervaporation properties of fluoroalkylsilane (FAS) grafted ceramic membranes", *Desalination* , 205 (2007)75–86.

Khayet, M., C. Cojocaru, M. Essalhi, "Artificial neural network modeling and response surface methodology of desalination by reverse osmosis", *J. Membr. Sci*., 368 (2011) 202-214.

Korin, E., I. Ladizhensky, E. Komgold, "Hydrophilic hollow fiber membranes for water desalination by the pervaporation method", *Chem. Eng. Process*., 35 (1996) 451-457.

Kuznetsov, Y.P., E.V. Kruchinina, Y.G. Baklagina, A.K. Khripunov, O.A. Tulupova, "Deep desalination of water by evaporation through polymeric membranes", *Russ. J. Appl. Chem.*, 80 (2007) 790-798

Lawson, K.W. and D.R. Lloyd, "Membrane distillation", *J. Membr. Sci*., 124 (1997) 1-25.

Li, L., N. Liu, B. McPherson, R. Lee, "Enhanced Water Permeation of Reverse Osmosis through MFI-Type Zeolite membranes with high aluminum contents", *Ind. Eng. Chem. Res*., 46 (2007) 1584-1589.

Liang, B., K. Pan, L. Li, E.P. Giannelis, B. Cao, "High performance hydrophilic pervaporation composite membranes for water desalination", *Desalination*, 347 (2014) 199–206.

Liang, B., W. Zhan, G. Qi, S. Lin, Q. Nan, Y. Liu, B. Cao, K. Pan, "High performance grapheme oxide/polyacrylonitrile composite pervaporation membranes for desalination applications", *J. Mater. Chem*., A 3 (2015) 5140-5147.

Lin, C., P. Ding, S. Smart, J.C. Diniz Da Costa, "Cobalt oxide silica membranes for desalination", *J. Colloid Interface Sci*., 368 (2012) 70-76.

Mujiburohman M., "Studies on pervaporation for aroma compound recovery from aqueous solutions", Ph.D. thesis, University of Waterloo, Waterloo, Ontario, Canada, 2008.

Naim, M., M. Elewa, A. El-shafei, "Desalination of simulated seawater by purge-air pervaporation using an innovative fabricated membrane", *Water Sci. Technol*., 72 (2015) 785-793.

Nguyen, Q.T., Y. Germain, R. Clement, Y. Hirata, "Pervaporation, a novel technigue for the measurement of vapor transmission rate of highly permeable films", *Polym. Test*., 20 (2001) 901-911.

Okada, T. and T. Matsuura, "A new transport model for pervaporation" *J. Membr. Sci*., 59 (1991)133–149.

Petersen, R.J., "Composite reverse osmosis and nanofiltration membranes", *J. Membr. Sci*., 83 (1993) 81-150.

Pislor, E., M. Alignan, P.Y. Pontalier, S. Grange, "Haemodialysis water production by double reverse osmosis", *Desalination*., 267 (2011) 88-92.

Potreck, J., K. Nijmeijer, T. Kosinski, M. Wessling, "Mixed water vapor/gas transport through the rubbery polymer Pebax® 1074" *J. Membr. Sci*., 338 (2009) 11-16.

Quiñones-Bolaños, E., H. Zhou, R. Soundararajan, , L. Otten, "Water and solute transport in pervaporation hydrophilic membranes to reclaim contaminated water for micro-irrigation", *J. Membr. Sci*., 252 (2005) 19-28.

Rao, S.M., "Reverse osmosis", *Resonance,* 16 (2011) 1333-1336.

Sabzi, F., M.R. Talaghat, A. Hosseini, "Prediction of water vapor sorption in the polymeric membranes using PHSC equation of state", *J. Natural Gas Sci. Eng*., 21 (2014) 757-763.

Sander, U. and P. Soukup, "Design and operation of a pervaporation plant for ethanol dehydration", *J. Membr. Sci*., 36 (1988) 463-475.

Sijbesma, H., K. Nymeijer, R. van Marwijk, R. Heijboer, J. Potreck, M. Wessling, "Flue gas dehydration using polymer membranes". *J. Membr. Sci*., 313 (2008) 263-276.

Singh, P.S., S.G. Chaudhri, A.M. Kansara, W. SSchetieger, T. Selvam, S. Reuss, V. Kaswal, "Cetyltrimethylammonium bromide-silica membrane for seawater desalination through pervaporation", *Bull. Mater. Sci*., 38 (2015) 565-572.

Shepherd, A., A.C. Habert, C.P. Borges, "Hollow fibre modules for orange juice aroma recovery

using pervaporation", *Desalination*., 148 (2002) 111-114.

Shieh, J.J. and R.Y.M. Huang, "A pseudophase-change solution-diffusion model for pervaporation II Binary mixture permeation", *Sep. Sci. Technol*., 33 (1988) 933-957.

Streicher, C., P. Kremer, V. Tomas, A. Hubner, G. Ellinghorst, "Development of new pervaporation membranes, systems and process to separate alcohols/ethers/hydrocarbons mixtures", in: R. Bakish (Ed.), *Proc. 7th Int. Conf. Pervaporation Proc. in Chem. Ind*., Bakish Material Corporation, Englewood, NJ, 1995, pp. 297-309.

Villaluenga, J.P.G., M. Khayet, P. Godino, B. Seoane, J.I. Mengual, "Pervaporation of Alcohols and Methyl tert-Butyl Ether through a dense poly (2,6-dimethyl-1,4-phenylene oxide) Membrane", *Ind. Eng. Chem. Res*., 43 (2004) 2548.

Wang, L., J. Li, Y. Lin, C. Chen, "Separation of dimethyl carbonate/methanol mixtures by pervaporation with poly(acrylic acid)/poly(vinyl alcohol) blend membranes", *J. Membr. Sci*., 305 (2007) 238-246.

Wang, N., L. Wang, R. Zhang, J. Li, C. Zhao, T. Wu, S. Ji, "Highly stable "pore-filling" tubular composite membrane by self-crosslinkable hyperbranched polymers for toluene/*n*-heptane separation", *J. Membr. Sci*., 474 (2015) 263-272.

Wangnick K., "1998 IDA worldwide desalting plants inventory", Wangnick Consulting GMBH, Germany, Report No. 18, 1998.

Wnuk, R. and H. Chmiel, "Direct heating of composite membranes in pervaporation and gas separation processes", *J. Membr. Sci*., 68 (1992) 293-300.

Won. W., "Separation of Dimethyl Carbonate/Methanol/Water Mixtures by Pervaporation Using Chitosan Membranes", MASc thesis, University of Waterloo, Waterloo, Ontario, Canada, 2002.

Wu, D., J. Martin, J. Du, Y. Zhang, D. Lawless, X. Feng, "Thin film composite membranes comprising of polyamide and polydopamine for dehydration of ethylene glycol by pervaporation", *J. Membr. Sci*., 493 (2015) 622-635.

Xu, J., C. Gao, X. Feng, "Thin-film-composite membranes comprising of self-assembled polyelectrolytes for separation of water from ethylene glycol by pervaporation", *J. Membr. Sci*., 352 (2010) 197-204.

Xie, Z., M. Hoang, T. Duong, D. Ng, B. Dao, S. Gray, "Sol-gel derived poly(vinyl alcohol)/maleic acid/silica hybrid membrane for desalination by pervaporation", *J. Membr. Sci*., 383 (2011) 96-103.

Zwijnenberg, H.J., G.H. Koops, M. Wessling, "Solar driven membrane pervaporation for desalination processes", *J. Membr. Sci*., 250 (2005) 235-246.

Appendix A

A.1 Sample calculations

Water permeation flux

The water permeation flux was calculated from the following data:

Feed: NaCl-H_2O

Effective membrane area (A): 22.05 cm^2

Operating temperature: 25℃

Time interval (t): 1 h

Quantity of permeate collected (M): 2.503 g

NaCl concentration in feed (C_f): 10000 mg/L

NaCl concentration in permeate (C_p): 3.5 mg/L

Water permeation flux: $J = \frac{M}{At} = \frac{2.503}{22.05\times10^{-4}\times1}$ =1135 g/(m^2.h)

Salt rejection

$$R = \frac{C_f - C_p}{C_f} \times 100\% = \frac{10000 - 3.5}{10000} \times 100\% = 99.97\%$$

Membrane permeance

The permeance of water was calculated from the following data:

Feed: NaCl-H_2O

NaCl concentration in feed (C_f): 10000 mg/L

Operating temperature: 298.15 K

Pereamtion flux of water (J_w): 1159 g/(m^2.h)

Saturated vapor pressure of water at 298.15 K (p_w^{sat}): 3.169 kPa

Mole fraction of water in feed (X_{w0}): 0.996902

Activity coefficient of water (γ_w): 1.000472 (Predicted by Aspen Plus)

Permeate vapor pressure of water (p^p): $\approx$0 kPa

Mole fraction of water in permeate (Y_i): 0.999568

The permeance of water:

$$\frac{P_w}{l} = \frac{J_w}{X_w \gamma_{iw} p_w^{sat} - Y_w p^p} = \frac{\frac{1135}{18}}{3.169 \times 0.996902 \times 1.000472} = 19.97 \text{ mol/(m}^2\text{.h.kPa)}$$

Activation energy

The temperature dependencies of permeation flux and membrane permeance can be expressed by the Arrhenius equation, and the apparent activity energy based on permeation flux (E_J) and the activity energy of permeation (E_P) can be obtained from the slopes of (ln J) vs (1/T) and [ln (P_i/l)] vs (1/T), respectively.

$$\ln J = \ln J_0 - \frac{E_J}{RT} \quad \text{(A2.1)}$$

$$\text{Slope}_1 = -E_J/R \quad \text{(A2.2)}$$

$$\ln(P_i/l) = \ln(P_{i0}/l) - \frac{E_P}{RT} \quad \text{(A2.3)}$$

$$\text{Slope}_2 = -E_P/R \quad \text{(A2.4)}$$

The apparent activity energy of water based on permeation flux (E_J), the activity energy of permeation (E_P), and the slope were calculated from the following data*

Temperature(℃)	Water flux [mol/(m^2.h)]	Permeance [mol/(m^2.h.kPa)]
25	63.06	19.97
35	68.06	12.15
45	74.39	7.80
55	81.94	5.23
65	89	3.58

*Feed of NaCl solution: 1 wt%

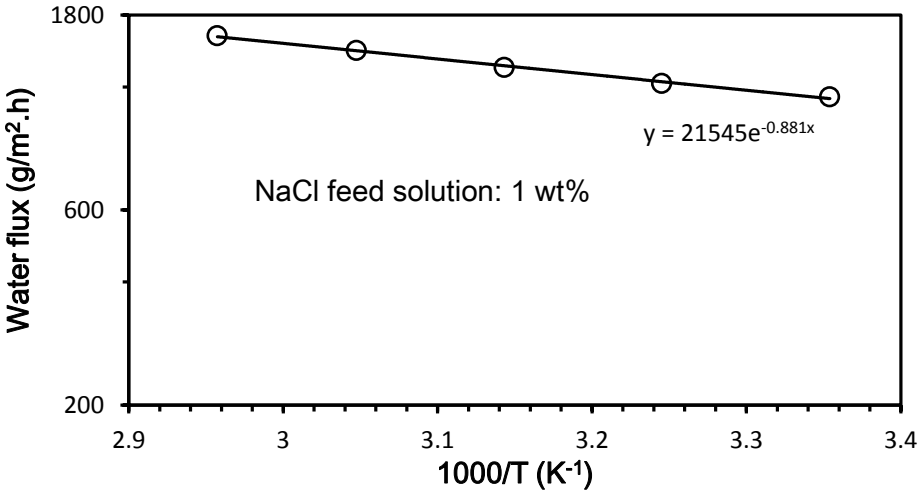

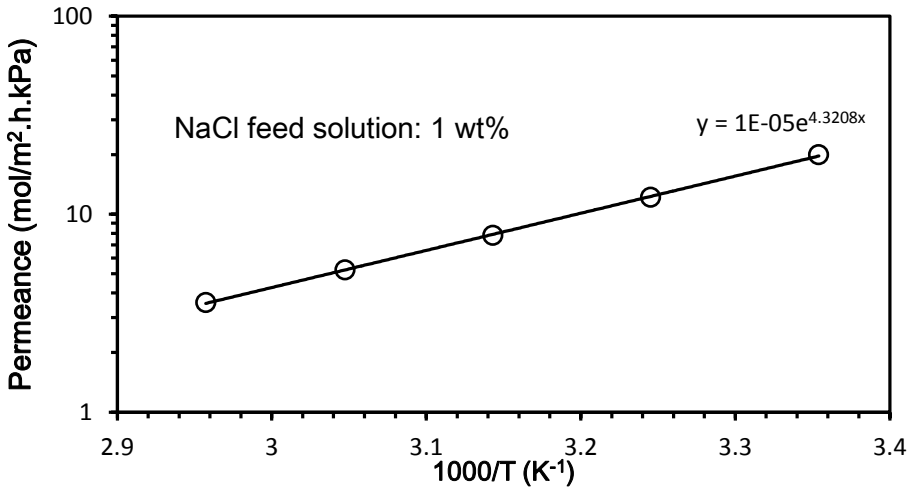

$Slope_1 = -0.881$ $E_J = -(-0.881 \times 8.314) = 7.32$ kJ/mol

$Slope_2 = 4.3208$ $E_P = -(4.3208 \times 8.314) = -35.92$ kJ/mol

The slopes of the Arrhenius plot for other salts are:

Compounds	Salt concentration (wt%)	$Slope_1$	$Slope_2$
Pure water	0	0.938	4.27
NaCl wt% in solution	1	0.881	4.321
	5	0.885	4.315
	10	1.094	4.103
	15	1.294	3.903
	20	1.208	3.993
Na_2SO_4 wt% in solution	1	0.905	4.297
	5	0.94	4.26
	10	1.094	4.1
	15	1.204	3.987
	20	1.217	3.975
$MgCl_2$ wt% in solution	1	0.835	4.366
	5	0.832	4.365
	10	1.158	4.056
	15	1.38	3.921
	20	1.424	3.885

A.2 Activity coefficients and saturated vapor pressure of water

The activity coefficient and saturated vapour pressure of water at different temperatures and salt concentrations were estimated using Aspen.

Compounds	Temperature (℃)	Salt concentration (wt%)	Activity coefficient of water	Saturated vapor pressure of pure water (kPa)
Pure water	25	0	1	3.169
	35	0	1	5.63
	45	0	1	9.590
	55	0	1	15.752
	65	0	1	25.022
NaCl solution	25	1	1.001	3.166
		5	1.002	3.089
		10	0.998	2.974
		15	0.987	2.835
		20	0.969	2.672
	35	1	1.001	5.617
		5	1.002	5.481
		10	0.998	5.276
		15	0.987	5.029
		20	0.968	4.739
	45	1	1.001	9.590
		5	1.001	9.565
		10	0.998	9.334
		15	0.987	8.983
		20	0.968	8.561
	55	1	1.001	15.752
		5	1.001	15.704
		10	0.997	15.319
		15	0.986	14.743
		20	0.968	14.049
	65	1	1.001	13.244
		5	1.001	25.022
		10	0.997	24.929
		15	0.987	24.318
		20	0.968	23.402

Activity coefficients and saturated vapor pressure of water (continued)

Compounds	Temperature (℃)	Salt concentration (wt%)	Activity coefficient of water	Saturated vapor pressure of pure water (kPa)
Na_2SO_4 solution	25	1	1.001	3.175
		5	1.008	3.146
		10	1.019	3.114
		15	1.029	3.070
		20	1.033	3.004
	35	1	1.001	5.633
		5	1.008	5.582
		10	1.019	5.522
		15	1.028	5.441
		20	1.032	5.322
	45	1	1.001	9.594
		5	1.008	9.506
		10	1.018	9.401
		15	1.027	9.261
		20	1.031	9.058
	55	1	1.001	15.747
		5	1.008	15.601
		10	1.018	15.424
		15	1.027	15.194
		20	1.031	14.865
	65	1	1.001	24.998
		5	1.008	24.764
		10	1.018	24.482
		15	1.027	24.118
		20	1.031	23.605

Activity coefficients and saturated vapor pressure of water (continued)

Compounds	Temperature (℃)	Salt concentration (wt%)	Activity coefficient of water	Saturated vapor pressure of pure water (kPa)
$MgCl_2$ solution	25	1	1.002	3.171
		5	1.010	3.123
		10	0.998	2.990
		15	0.949	2.748
		20	0.870	2.425
	35	1	1.002	5.627
		5	1.010	5.541
		10	0.999	5.310
		15	0.953	4.896
		20	0.877	4.341
	45	1	1.002	9.583
		5	1.010	9.434
		10	0.999	9.051
		15	0.957	8.366
		20	0.884	7.449
	55	1	1.002	15.729
		5	1.010	15.482
		10	1.000	14.862
		15	0.959	13.771
		20	0.890	12.306
	65	1	1.002	24.968
		5	1.009	24.570
		10	1.001	23.599
		15	0.962	21.910
		20	0.895	19.645